Geosphere

Holocene paleo-earthquakes recorded at the transfer zone of two major faults: the Pastores and Venta de Bravo faults (Trans-Mexican Volcanic Belt)

--Manuscript Draft--

Manuscript Number:	GS1071R1
Full Title:	Holocene paleo-earthquakes recorded at the transfer zone of two major faults: the Pastores and Venta de Bravo faults (Trans-Mexican Volcanic Belt)
Short Title:	Holocene paleo-earthquakes in the Trans-Mexican Volcanic Belt
Article Type:	Research Paper
Keywords:	Seismic hazard, paleoseismology, Acambay graben, neotectonics, central Mexico
Corresponding Author:	Gerardo J Aguirre-Diaz, PhD Centro de Goeciencias, Universidad Nacional Autónoma de México UNAM Querétaro, Querétaro MEXICO
Corresponding Author Secondary Information:	
Corresponding Author's Institution:	Centro de Goeciencias, Universidad Nacional Autónoma de México UNAM
Corresponding Author's Secondary Institution:	
First Author:	María Ortuño, Dr.
First Author Secondary Information:	
Order of Authors:	María Ortuño, Dr.
	Francisco Ramón Zúñiga, Dr.
	Gerardo J Aguirre-Diaz, PhD
	Dora Carreón-Freyre, Dr.
	Mariano Cerca, Dr
	Matteo Roverato, Ddr
Order of Authors Secondary Information:	
Abstract:	We present evidence of five late Holocene earthquake ruptures observed at two paleoseismological trenches in the Laguna Bañí sag- pond. The trenches exposed two fault branches of the western termination of the Pastores fault, one of the major fault systems within the Central Trans-Mexican Volcanic Belt. The site was studied by combining geomorphological and structural approaches, volcanic mapping, ground penetrating radar and paleoseismological analysis. The study revealed that co-seismic surface rupture was non-characteristic and that the exposed fault branches not always moved simultaneously. The fault tip has ruptured at least five times within the last 4 ka and the rupturing events followed and preceded the deposition of an ignimbrite. The close temporal relationship of the seismic rupture with the volcanic activity of the area could be the result of volcanism triggered by faulting and its associated seismicity. The relatively high recurrence of seismic events (1.1-2.6 ka) and the non-characteristic fault behavior observed at this tip of the Pastores fault suggest, 1) that the fault might have been active as a primary fault rupturing along segments of variable length or depth, and/or 2) that the fault ruptured eventually as a secondary fault. The secondary ruptures would likely be related to earthquakes produced at major neighboring faults such as the Acambay fault, which moved during the 1912 Acambay earthquake, or the Venta de Bravo fault. A relatively large slip rate estimated for this fault branch (0.23 - 0.37 mm/yr) leads to contemplate the possible on depth connection between the Pastores and the Venta de Bravo faults, increasing the maximum expected magnitude for Central Mexico.

Answer to comments

Click here to download Cover Letter: Ortuno et al Answer to comments.pdf

Holocene paleo-earthquakes recorded at the transfer zone of two major faults: the Pastores and Venta de Bravo faults (Trans-Mexican Volcanic Belt)

María Ortuño[1, 2], F. Ramón Zúñiga[1], Gerardo J. Aguirre-Díaz[1], Dora Carreón-Freyre[1], Mariano Cerca[1], Matteo Roverato[1, 3]

[1] *Centro de Geociencias, Universidad Nacional Autónoma de México, Blvd. Juriquilla, 3001, 76230, Juriquilla, Querétaro, México*

[2] *Dept. de Geodinàmica i Geofísica, Universitat de Barcelona, c/Martí i Franquès s/n, 08028, Barcelona, Spain.*

[3] *IGC Instituto de Geociências, Universidade de São Paulo, Rua do Lago, 562 Cidade Universitária 05508080 - São Paulo, SP - Brasil*

Geosphere, version of September 8, 2014

ABSTRACT

We present evidence of five late Holocene earthquake ruptures observed at two paleoseismological trenches in the Laguna Bañí sag- pond. The trenches exposed two fault branches of the western termination of the Pastores fault, one of the major fault systems within the Central Trans-Mexican Volcanic Belt. The site was studied by combining geomorphological and structural approaches, volcanic mapping, ground penetrating radar and paleoseismological analysis. The study revealed that co-

seismic surface rupture was non-characteristic and that the exposed fault branches not always moved simultaneously. The fault tip has ruptured at least five times within the last 4 ka and the rupturing events followed and preceded the deposition of an ignimbrite. The close temporal relationship of the seismic rupture with the volcanic activity of the area could be the result of volcanism triggered by faulting and its associated seismicity. The relatively high recurrence of seismic events (1.1-2.6 ka) and the non-characteristic fault behavior observed at this tip of the Pastores fault suggest, 1) that the fault might have been active as a primary fault rupturing along segments of variable length or depth, and/or 2) that the fault ruptured eventually as a secondary fault. The secondary ruptures would likely be related to earthquakes produced at major neighboring faults such as the Acambay fault, which moved during the 1912 Acambay earthquake, or the Venta de Bravo fault. A relatively large slip rate estimated for this fault branch (0.23 – 0.37 mm/yr) leads to contemplate the possible on depth connection between the Pastores and the Venta de Bravo faults, increasing the maximum expected magnitude for Central Mexico.

KEYWORDS: Seismic hazard, paleoseismology, Acambay graben, neotectonics, central Mexico.

INTRODUCTION

In intra-continental regions, deformation rates of active faults are relatively low, so that recurrence periods of seismogenic ruptures occurring at a particular fault may exceed thousands of years (Stein and Liu, 2009). In these regions, the social perception of seismic hazard is lower than in active continental margins, which are frequently affected by destructive earthquakes every few decades. The low rate of

seismicity in intracontinental areas has led to an increasing use of the paleoseismological technique as an effective tool in identifying destructive earthquakes occurred in the past. It also provides additional data for a better determination of seismic hazard and, in some cases it is the only source of data towards this purpose (Joyner and Fumal, 1985; Masana et al., 2001, Stein and Liu, 2009). A frequent handicap in the paleoseismological research is the complexity of fault dynamics. In large normal fault systems it is frequent that faults are corrugated due to en echelon arrays or overlapping segments that might move simultaneously during a seismic event (e.g., Ferrill et al., 1999). If extension is accounted by a large number of faults, the number of structures activated during an earthquake might be relatively high, either because they merge at depth or in relation to seismically induced effects (e.g., Beanland et al., 1989, McCalpin, 2009). The activity of faults as secondary structures during the rupture of a major fault has been reported in numerous scenarios (e.g., King et al., 1994, Berberian et al., 2001). The rupture of the Madison fault during the 1959 Hebgen lake earthquake (Witkind et al., 1962) or that of the Laguna Salada fault during the 2010 Sierra Cucapah earthquake (Fletcher et al., 2014) are some examples of coseismic slip (<< 1 m) in faults that are neighbors of a major rupturing structure. Thus, when recorded in the geology, the earthquake chronology associated to a given fault might reflect its activity as a main seismogenic fault, but also as a secondary structure. This aspect can be regarded as a disadvantage but also as the opportunity to find synthetic records of seismic events experienced at a given area, independently of the fault that have generated them.

The central region of Mexico is an example of an intra-continental zone in which the activity of faults has led to historical destructive earthquakes. Examples are the earthquakes of 1568 in the Chapala graben (M ~ 7; Suárez et al., 1994) and of 1875 at Jalisco (M ~ 7.1; García-Acosta and Suárez, 1996), or the recent earthquakes at Acambay of 1912 (Ms = 6.7; Suter et al., 1996), and at Jalapa, 1920 (m_b = 6.9; Suárez, 1992). All these earthquakes were produced by faults located within the Trans-Mexican Volcanic Belt (TMVB), which is a Middle Miocene to Quaternary arc related to the subduction of the Cocos and Rivera plates beneath the North American plate (Demant, 1978; Nixon, 1982, Aguirre-Díaz et al., 1998; Siebe et al., 2006; Ferrari et al, 2012; **Fig. 1**). Some of the largest cities in Mexico (e.g., Mexico City,

Guadalajara, Toluca, Querétaro) are within this region and because they are located above or near active faults, with the added factor of abnormal amplification of seismic waves (Ovando-Shelley et al., 2012), a large proportion of Mexico's population is at significant risk of suffering earthquake damage. Thus, seismic risk plans should be well established, incorporating well-constrained seismic hazard parameters based on reliable geological data.

This paper focuses on the activity of the Pastores fault, the southern boundary of the Acambay graben and one of the most active faults of the TMVB (Suter et al., 1991, 1992, 2001; **Figs. 2 and 3**), with seismogenic behavior revealed through the study of paleoseismological trenches at its eastern tip (Langridge et al., 2013). Besides moving as a primary seismogenic source, the activity of this fault as a secondary structure of the Acambay fault has been inferred by Suter et al., (1996, 2001) on the basis of the earthquake effects of the 1912 Acambay earthquake reported by Urbina and Camacho (1913). Moreoever, the linkage between the Pastores fault and the Venta de Bravo fault, the larger fault in the Acambay graben, has also been considered in several previous works (e.g., Suter et al., 1992, 2001; Langridge et al., 2013). These two faults are aligned and form the southern boundary of the Acambay graben. The Pastores fault western termination overlaps the Venta de Bravo fault along a 14-15 km zone. The study of this area is thus relevant for the evaluation of the activity as a transfer zone between two major systems that might be linked at depth, implying a significant seismic hazard.

The main objective of our study is to search for the evidence of Holocene earthquake ruptures at the westernmost Pastores Fault Zone, characterizing the tectonic style and establishing a paleo-earthquake chronology that could help to better understand its linkage with the Acambay and the Venta de Bravo faults. For this purpose, we rely on neotectonic techniques and ground penetrating radar prospection (see **Appendix A.1** for details on the applied methods). The understanding of the late Quaternary evolution of the area was possible by the elaboration of a map containing the main tectonic structures, landforms and geological materials, which allow us to discuss the geological significance of the paleoearthquakes detected. With the paleoseismological and volcanic data shown here, we aim at improving estimates of

seismic and volcanic hazard for this area and ultimately help to mitigate the natural hazards to which the population is exposed.

GEOLOGICAL AND GEOMORPHOLOGICAL SETTING

The TMVB traverses the center of Mexico from the Pacific Coast to the Gulf of Mexico (**Fig. 1**). According to some authors (e.g., Pardo and Suárez, 1995; Gomez-Tuena et al., 2005), the obliquity of TMVB with respect to the Mesoamerican trench is directly related to differences in the angle of the subducting plate. This angle reaches 70º in the central and western part of the arc and it is locally very low (near 25º) at the easternmost part, as revealed by the analysis of the seismicity along the subduction zone (Pardo and Suárez, 1995; León-Soto et al. 2009) and by geophysical transects such as gravimetric or seismic tomography (Urrutia-Fucugauchi and Flores-Ruiz, 1996; Rogers et al., 2002; Pérez-Campos et al., 2008; Husker and Davis, 2009; Yang et al., 2009; Stubailo et al., 2012). The structure and kinematic of faults in the TMVB have been studied by many authors who have addressed them regionally (e.g., Pasquaré et al., 1987; De Cserna, 1989; Aguirre-Díaz et al., 1998; Ferrari et al., 2012), or focused on the observed deformation at specific regions (e.g., Suter et al., 1992, 2001; Langridge et al., 2000; Aguirre-Díaz et al., 2005; Norini et al. 2006).

Neotectonic activity along the TMVB can be divided into three geographical zones with distinctive volcanism and structural features: the western, central and eastern sectors (Pasquaré et al. 1987, Aguirre-Díaz et al., 1998; García-Palomo et al. 2000). The Pastores fault is located in the central part of the TMVB, which is constituted by a complex mosaic of horsts and grabens and extends from Guadalajara City to Mexico City valley (**Fig. 1;** Aguirre-Díaz, 1996; Aguirre-Díaz et al., 1998). The central part of the TMVB had been referred as the Chapala-Tula fault system by Johnson and Harrison (1990). Regional extensional and transtensional kinematics of this zone since the Miocene is well documented (Johnson and Harrison; 1989, Martinez-Reyes and Nieto-Samaniego, 1990; Garduño et al., 2009), and a minor left-lateral component in the overall extension has been identified (Suter et al., 1992;

1995; 2001; Ramírez-Herrera et al., 1994; Ramírez-Herrera, 1998; Ego and Ansan, 2002; Norini et al. 2006). According to Suter et al. (1995, 2001) and to Ego and Ansan (2002), the central TMVB has been dominated by transtensive stresses since the Middle Quaternary, with σ_3 oriented NW-SE. Besides this E-W intra-arc fault system there is a NW-trending fault system named Taxco-San Miguel de Allende, which lies between near Querétaro city in the NW and Taxco in the SE (Demant, 1978; Aguirre-Díaz et al., 2005; Alaniz-Alvarez and Nieto-Samaniego, 2005), also named as the Querétaro Fault System (Johnson and Harrison, 1990). This fault system coincides with a change in the regional crustal thickness and marks a gradient in the regional gravity anomaly of central Mexico, thus representing an important crustal discontinuity (Aguirre-Díaz et al., 2005). It passes through the central part of the Acambay graben at depth, marked by an alignment on some volcanic structures and a change in the width of the graben (Suter et al., 1991; 1995; Aguirre-Díaz, 1996).

Paleoseismicity and seismicity in the Central TMVB

The Acambay graben is located at the central-eastern part of Central TMVB (**Fig. 2**). The faults identified in the central TMVB have an approximate EW trend and mainly affect Neogene and Quaternary cinder cones, domes and lava bodies (basaltic, andesitic and rhyolitic), as well as pyroclastic deposits (Suter et al., 1991; Aguirre-Díaz, 1995, 1996; Aguirre-Díaz et al., 2000; Garduño et al., 2009; Ferrari et al., 2012). The faults also affect Cretaceous metamorphic rocks in some regions(**Fig. 3**; Suter et al., 1991, 1992; Aguirre-Díaz, 1995, 1996); and to a lesser extent, Plio-Quaternary lacustrine and fluvial deposits which fill the recent tectonic depressions (e. g., Suter et al., 1991, 1992, 1995; Ramírez-Herrera et al., 1994; Ramírez-Herrera, 1998; Aguirre-Díaz et al., 2000; Langridge et al., 2000; Garduño et al., 2009; Rodríguez-Pascua et al., 2010).

In the Central TMVB, nearly 100 faults with a trace larger than 2 km are characterized by having geomorphological expression, with steep multi-event scarps. Among them, 65 faults displace rocks of known Quaternary age and have vertical slip

rates that range between 0.2 and 0.02 mm/yr, the age of the rest of the faults not being well constrained so far. Minor lateral displacements have been observed in some E-W trending structures (Suter et al., 2001). Further slip rates have been provided for the Acambay fault at 0.17 ± 0.02 mm/yr (Langridge et al., 2000) and for the Pastores fault, which moves at 0.03 - 0.04 mm/yr vertical rates near its intersection with the Lerma River (Suter et al., 1992; Langridge et al., 2013). Due to the scarcity of available ages and to the lack of palaeoseismological studies, Suter et al. (2001) distinguish only four faults with proven activity during the late Quaternary-Holocene in the Central TMVB. These are the Acambay, Pastores, Temascalcingo and Morelia faults (**Fig. 2**). Ramírez-Herrera (1998) also considered the Venta de Bravo fault as being active during the Late Quaternary on the basis of morphometric indexes such as sinuosity or the development of triangular facets and scarp dissection (**Figs. 2** and **3**).

The Acambay graben is bounded to the north by the Acambay-Tixmadejé fault and to the south by the Pastores and Venta de Bravo faults. It is dissected at its central part by the Central-graben fault system, with the Temascalcingo fault as the most conspicuous one. Other faults can be recognized on the surface indicating recent activity based on cutting relationships (**Fig. 3**). The Pastores fault neotectonic activity has been previously documented by several authors (e.g., Suter et al. 1995, 2001; Ramírez-Herrera et al, 1998; Persaud et al., 2006; Langridge et al., 2000, 2013). The fault affects volcanic rocks of Miocene age as well as alluvial terraces on the banks of Lerma River (**Fig. 4**). Trench excavations by Langridge et al. (2013) at one of the branches of the fault showed a succession of lacustrine sediments (1σ calibrated age of 41-34 ky BP), tilted 7 º to the north, and covered by pyroclastic flow and fall deposits, and more recently, slope deposits. Lacustrine deposits affected by faulting have also been observed in natural outcrops at the foot of the escarpment by Ramírez-Herrera (1998) and Suter et al. (1995).

Paleoseismological studies on faults in Mexico concentrate in the Central TMVB. Three of these studies are located in the eastern part of this region, including Langridge et al. (2000) in the Tixmadejé-Acambay fault, Langridge et al. (2013) in the central-eastern part of the Pastores fault, and Ortuño et al. (2011) in the central

faults of the Acambay graben (**Fig. 3**). Other studies are focused in the western part, including Rodríguez-Pascua et al. (2004) on Lake Patzcuaro (nearly 50 km to the west of Morelia), and Garduño et al. (2009) on La Paloma fault, which traverses the City of Morelia (**Fig. 2**). These studies have reported fault displacements from earthquakes that occurred in pre-Columbian times (Rodríguez-Pascua et al., 2004; Garduño et al., 2009) as well as in the twentieth century (the 1912 Acambay earthquake, Langridge et al., 2000).

The Acambay earthquake (November 19, 1912, Ms = 6.7, Suter et al., 1996) is the only instrumental earthquake in the TMVB with known associated surface rupture. During this event, three faults seem to have broken the surface as described by Urbina and Camacho (1913), the Acambay-Tixmadejé fault (main fault with a maximum displacement of 50 cm), Temascalcingo fault (with a maximum displacement of 30 cm), and the Pastores fault. It is not clear if this latter fault ruptured co-seismically the surface during this event or it only showed open fractures along its trace; from the descriptions compiled by Urbina and Camacho (1913), Suter et al. (1995) estimated surface rupture lengths of 41 km and 20 km lengths for the Acambay-Tixmadejé and Temascalcingo faults, respectively, and inferred the formation of a 17 km long scarp of unspecific height along the trace of Pastores fault. However, according to the paleoseismic data of Langridge et al. (2000, 2013) on two trenches excavated on the eastern tip of Pastores fault, the fault did not rupture the surface on the 1912 earthquake.

The palaeoseismological study of the Acambay-Tixmadejé fault enabled Langridge et al. (2000) to identify four Holocene ruptures with an average dip displacement of 60 cm per event, a recurrence period of 3,600 yrs and an average vertical slip rate of 0.17 ± 0.02 mm/yr. Moreover, the work of Langridge et al. (2013) on the Pastores fault showed no Holocene deformation, although they found three paleoseismic events with a minimum displacements of 35-50 cm occurring at 31.5-41 cal. kyr BP, at 23.9 – 34.6 cal. kyr BP and at 12.2 – 12.6 cal. kyr BP. Paleoseismological studies by Rodríguez-Pascua et al. (2010) indicate that the area has experienced at least five earthquakes of Mw > 5 that affect Pleistocene lake sediments located at the foot of the Pastores fault. Besides the Acambay earthquake

of 1912 other known pre-instrumental earthquakes with intensities larger than VI occurred in the Cuitzeo and Venta de Bravo regions (Orozco and Berra, 1887; Suter et al. 1992; García-Acosta and Suarez, 1996). The instrumental analysis of seismicity for the years 1969 - 1992 in the central part of TMVB led Suter et al. (2001) to recognize that most of the epicenters fall in the western segment of the graben, which is bounded by the Epitacio Huerta and Venta de Bravo faults. The only focal mechanism determined for instrumental earthquakes in the region is that of the Maravatío earthquake (2/22/1979). This earthquake had an m_b = 5.3, epicentral location N of the Venta de Bravo fault and corresponds to a focal mechanism with nodal planes showing normal faulting with lateral component in EW and NE-SW oriented planes (Astiz, 1980; Ego and Ansan, 2002; **Fig. 2**). Two medium size earthquakes (Mc = 3.8 and 3.7) took place near the town of Maravatío on February 8 and March 15 2013. Even though the focal mechanisms are not well constrained, they are consistent with a NS extension which agrees with that of the 1979 event. Location of the epicenter and of intensity distribution of the main shock suggest the Venta de Bravo fault as the seismogenic source of this earthquake. Kinematic data from geological observations along this fault are in agreement with the left lateral slip component observed in the focal mechanism (Suter et al., 1992).

STRUCTURAL AND GEOMORPHOLOGICAL FEATURES

The Pastores fault

The Pastores fault is one of the most active faults within the Acambay graben according to its geomorphological expression (**Figs. 3, 4, 5** and **6**). Its rectilinear trace extends along 32 km and can be differentiated in two segments, the eastern (11.5 km) and the western (20.4 km) segments. The eastern segment goes from the Lerma River north of Atlacomulco to the western end of San Andres range (**Fig. 3**), with a variable scarp height reaching a maximum value of 200 m. The fault mainly affects Miocene dacitic lavas and block and ash flow deposits of a north-south trending lava dome range between Acambay and Atlacomulco, and Plio-Quaternary dark grey, aphanitic

andesitic lavas with platy-jointing and/or vesicular blocky structure. The vents of these lavas are not defined, but by the ramp structures observed in some of them, it is possible that their vents are located to the south of the Pastores fault. This part of the fault has several secondary faults developed on the hanging wall as well as rear scarps of probable gravitational origin affecting the slopes of the Maye mountain range (**Fig. 3**).

The western segment of the Pastores fault (WPF) extends from the Lerma River to Canchesdá. Its trace is continuous and gradually increases towards the middle part of the scarp, reaching a height of 120 m (**Figs. 4** and **5**). The fault affects Pliocene dacitic lava domes (Bañí lava domes) and Plio-Quaternay aphanitic, dark grey, andesitic lavas, which are interbedded with lahar deposits rich in blocks of dark grey andesite and grey porphyritic dacite. The more linear trace of the WPF and the lower scarp height could be explained by the relatively younger age of the volcanic material affected, which is consistent with the poor development of the fluvial network at the uplifted southern block compared to the Eastern Pastores fault (EPF). The area between the Pastores and Venta de Bravo fault is occupied by a sag pond, interpreted by several authors (e.g., Suter et al., 1991, 1992, 2001; Ramirez-Herrera, 1998) as indicative of a left-lateral component in the slip of the faults. As already suggested by other authors (e.g., Suter et al., 1992, 1995, 2001), we suspect that the Pastores and Venta de Bravo faults could be linked at depth in a more complex system, that is, the Venta de Bravo-Pastores fault system (**Fig. 3**). Contrarily, Langridge et al. (2013) have considered unlikely that these faults could act as a single seismogenic fault source owed to the hypothetical presence of a crustal major boundary in the relief zone, the Taxco-San Miguel de Allende Fault Zone, and to the fact that this area matches with the western end of the surface rupture during the 1912 Acambay earthquake. This issue would be readdressed in the Discussion.

The Pastores western termination and the Laguna Bañí pull-apart basin

The western termination of the WPF cannot be straightforward defined based on its geomorphological trace. Some authors (e.g., Langridge et al., 2000;

2013) have considered that the Pastores fault has a single trace, with a bend towards the south at its western tip (next to its intersection with the Mexico-Guadalajara highway). We interpret that the WPF ends towards the west into a splay of two faults, the southern WPF (that is, the trace defined by Langridge et al., 2013) and the northern WPF, which is in continuity with the main trace near Canchesdá and also bends to-the south few kilometers to the west (**Figs. 4 and 5**). This type of splay has been observed at many normal faults systems (e.g., Bahat, 1981; Ferrill et al., 1999; Soliva et al., 2008) and is present at the termination of other faults within the graben, as those described by Suter et al. (1992) and Ramírez-Herrera (1998). A pull-apart basin has been associated to each of these bends. This basin is occupied nowadays by the Laguna Bañí lacustrine area, which is a natural pond occasionally drained on purpose for agricultural purposes (**Fig. 5**). The bended geometry of the fault trace is characteristic of many other E-W faults in the Central TMVB, and might be the result from the linkage of right stepping faults or from the interaction of E-W oriented faults with NNE-SSW pre-existing fractures (**Figs. 2**, **3**). Some other pull-apart basins and sag ponds have been identified in other neighboring sites, as it is the case of some of the Venta de Bravo faults bends and secondary fault segments (**Figs. 3, 4**).

We chose to locate the study within this area because it is one of the few places where the Pastores fault seems to affect rocks of Holocene age. The surface expression of the faults is very conspicuous because the volcanic rocks affected are highly resistant (for instance, lava flows and domes as well as welded scoria deposits and ignimbrites). This circumstance leads to an excellent preservation of the fault scarps, which maintain rectilinear traces through hundreds of thousands of years and make the faults easily detectable even in far-field satellite images (e.g., Johnson and Harrison, 1989). However, the same fact acts against the paleoseismological record due to the absence of sedimentary traps on top of the scarps. This absence has a double cause; 1) the low degradation rate affecting the resistant scarps does not allow the development of local low-lands on them, such as incised valleys or degraded scarps with associated piedmonts; 2) the absence of fine alluvial sediment supply that could cover the scarps; since the uplifted block is difficult to erode, no developed alluvial drainage is installed on it providing sorted sediment supply as alluvial fans. The most common recent rocks affected by fault activity in this setting are the slope

326 talus or colluvium deposits made up of coarse blocks falling from the free faces of the
327 scarps, which evolve as a retreating-type scarps. At some locations, volcanic fall or
328 flow deposits might be preserved. If affected, and when the thickness of the deposit is
329 not too high, these sites are appropriate to look for the paleoseismological record. In
330 such an environment, the small pull-apart basins generated in the fault bends are
331 exceptional localities in which we might found late Quaternary sediments affected by
332 the activity of the faults. Additionally, studying the tips of the faults is a further
333 alternative to the problem of having too high scarps; since the fault displacement is
334 smaller at those parts of the fault, there are more chances for the scarps being buried
335 after an earthquake (e.g., Ortuño et al., 2012). The Pastores fault western termination
336 at Bañí site meets these two conditions: it is a fault tip and coincides with a fault bend
337 associated to a pull-apart basin filled with recent lacustrine sediments. A main
338 evidence suggesting the continuity of the Pastores trace towards the west along the
339 northern WPF (that is, in the direction of the Laguna Bañí site) is the mapped rupture
340 of the 1912 Acambay earthquake as described by Urbina and Camacho (1913) and
341 revisited by Rodríguez-Pascua et al. (2012). Even though there is no report about the
342 displacement along this fault, open fractures were documented and mapped along the
343 western Pastores fault with a rupture extends across a low-land located next to
344 Santiago Cochochitlán (**Fig. 4**).

345

346 **Western Pastores fault exposures**

347 Several outcrops along the western end of the Pastores fault allow a direct
348 observation of the materials affected by the neotectonic activity of the fault and its
349 most relevant structural features (**Figs. 4, 5 and 6**). These observations are described
350 below as three distinct sites.

351 *Site A* (19º51'28''N, 100º01'52''W). It is located at the eastern margin of a
352 watercourse-oriented perpendicular to the Pastores fault, south of the Santiago
353 Cochochitlan locality (near Boquí town, **Fig. 4**). At the head of the watercourse, the
354 Pastores fault develops a fault breccia with a thickness of 1- 2 m on Pliocene lavas of
355 dacitic composition belonging to the Bañí lava domes unit. Fracturing in the footwall

lava has a decimetric spacing, yielding the aspect of a foliated rock. Fluvial-lacustrine sediments of apparent Pleistocene age (Aguirre-Díaz et al., 2000) are exposed in the hanging wall and are affected by secondary faulting. Fluvial conglomerate north of the lavas show a sub-vertical 2-3 m thick tectonic breccia. Discrete faults within this Fault Zone show *S-C* planes and sigmoid fault branches (**Fig. 6c**). Another fault is observed 20 m to the north along the watercourse displacing sub-horizontal layers of medium to coarse-grained conglomerates and fluvial silt. This fault shows striated fault planes (**Figs. 6d** and **f**). Fault planes measured trend N75E – N097E, dip between 50º to 70º towards the N, and contain slickenlines with a pitch of 50º to 65º W indicating NNW to NW extension (**Fig. 6c**). The data indicates extensional and left-lateral components of displacement with up to 1 m of throw affecting the fluvial materials, which is in agreement with previously structural data reported by Suter et al. (1995) in two neighboring outcrops of the WPF affecting Middle Pleistocene lavas.

Site B (19º51'34''N, 100º02'44''W). It is an artificial cut oriented N-S at the termination of the Pastores fault (**Fig. 6g**) that shows recent materials deposited on top of the fault scarp. At the base, there is a lahar deposit on top of pink volcanic ash deposits. A paleosoil has been preserved on top of the lahar unit. Overlain this paleosoil is a pyroclastic flow deposit. Talus detritus < 10 cm thick covers the sequence. No clear faults are observed in this outcrop, although some subsurface faulting is inferred from the geometry of the layers and the steps in present day surface (surface previous to the quarry). We did not find a clear surface scarp in the surroundings, but did notice that that some limits of agricultural crops run parallel to the fault trend, possibly because the fault has caused secondary fractures that are difficult to erase by farmers. One of these fractures has been locally widened and has been used as an agricultural drainage channel.

Site C (19º52'36''N, 100º03'42''W). It corresponds to the Laguna (lake) Bañí, which lies in a topographic depression located at the left step over of the northern WPF (**Figs. 4, 5 and 6b**). In this area, the hanging wall is occupied by a fluvial-lacustrine system interpreted here as a tectonic sag pong. The fluvial-lacustrine area is limited to the south by the fault, which is affecting tabular lava flows of dacitic composition

corresponding to low lava domes with flat tops and vertical margins, and to the north, by other dacitic domes of the same group. These dacitic lava domes, named informally as Bañí dacitic domes (**Fig. 3**), form a dome complex that extends across the central portion of the Acambay graben, between the volcanoes of Temascalcingo and Altamirano, and continue to the south beyond the Pastores fault. The fault also affects block and ash flow deposits identified along the scarp on top of Pliocene dacitic lava flows. In this site, the geometry of the fault trace shows a bend, which seems to result from the linkage of two faults that have a stepping geometry (**Fig. 5A**). A splay of faults is expected to have formed near the fault bend, causing a partition of the deformation of the surface along minor fault branches. The southern fault branches would be responsible of the main scarp, so they have been called as "Hill Fault branch, HFB" whereas the northern fault branches would be covered by lacustrine deposits so they have being called as "Lake Fault branch, LFB" (**Fig. 5B**). The HFB is mostly covered by trees and talus material, which makes it difficult to observe clear fault surfaces (**Fig. 6E**). Lavas and domes are Pliocene according to our mapping and based upon the stratigraphy of Aguirre-Díaz (1996) and Aguirre-Díaz et al. (2000). The fault scarp has a maximum height of 30 m and a maximum slope of 35-40% near the sag pond. Near the lacustrine area, two fan-like forms interpreted as debris cones, and a possible rear scarp on the up-thrown block, account for the lack of straightness of the fault trace. The base of the scarp towards the east is artificially modified by an irrigation channel following the fault trace (**Fig. 5A**). Although this area was not included in the mapping of geological effects of the 1912 Acambay earthquake by Urbina and Camacho (1913), the inhabitants of the area were told by their grandparents that a natural spring next to the lake stopped providing water right after that earthquake, which is interpreted here as evidence of co-seismic shaking.

PALEOSEISMOLOGICAL TRENCHES AT THE NORTHERN WPF. THE LAGUNA BAÑI SITE

Laguna Bañí site was selected for GPR prospecting and paleoseismological

trenching by the following reasons: **1)** the lacustrine area is a sedimentary depocenter facilitating a more complete geological record (e.g., burial and preservation of co-seismic displacements) than other sites in which the scarp is evident but erosive processes predominate; **2)** the lacutrine environment favors the accumulation of organic matter making possible the dating of the layers potentially affected by faulting; **3)** the expected fault splay geometry is appropriate for the study of a complete faulting chronology due to the partitioning of the deformation in different branches; **4)** since the area corresponds to the fault termination, smaller slip-per event displacements are expected, which are more easily buried than greater; **5)** we have considered that secondary faulting or crack opening during the 1912 Acambay earthquake might have occurred in the area based on the earthquake hydrological effects reported by the local people. Consequently, the site seems a good location to look for evidence of secondary co-seismic behavior of Pastores with respect to Acambay fault.

Two trenches were excavated in Laguna Bañí: Laguna East and Laguna West. Both trenches were oriented N-S, approximately perpendicular to the main trace of the northern WPF, and showed deformation along the Lake Fault branch (**Fig. 5B**). In this section, we describe the geological materials and the tectonic deformation affecting them, which was analyzed to obtain a paleo-earthquake chronology. The age of the events was constrained by the radiocarbon dating results summarized in **Table 1**. **Figures 7** and **8** show the stratigraphic record observed at the trenches and GPR profiles along with a detailed sedimentological description.

Laguna West trench

This trench was located in a higher position on the topographic scarp relative to the other trench (Laguna East; **Fig. 4**). The trench was 15 m in length, 2-3 m in depth, and 2 m wide. The trench exposed five colluvial deposits (C1-5) derived from the topographic scarp located to the south. These deposits are inter-layered with a pyroclastic flow deposit named Bañí ignimbrite, which thickens towards the north of the trench. The present-day soil (S.1) is developed on top of fine-grained colluvial

material (Fig. 7A and 7B). Bañí ignimbrite is massive, grey when fresh and brown in weathered zones, and it is mostly composed of ash, which supports grey pumices and a few small (<2 cm) lithics of andesite. Pumice clasts are angular, <2 cm in size. Pumice and matrix include plagioclase, hornblende, biotite and quartz. Based on this mineralogy, the composition should correspond to dacite or rhyolite, but it has not been chemically analyzed to confirm this. The ashy matrix has been replaced by brown clay at the base and top of the deposit due to weathering processes. The ignimbrite contains small charcoal clasts that were sampled for C-14 dating. The most probable volcanic sources of this ignimbrite are the Temascalcingo volcano or the Altamirano volcano (**Fig. 3**). Further geologic and geochronologic studies are needed to confirm which of these volcanoes produced the Bañí ignimbrite. The sequence is affected by three discrete faults cutting all units except for the upper soil (C.1 unit). These faults are oriented N097ºE – N088ºW with dips of 80 to 88º toward the N. Dip fault displacements, between 9 and 20 cm, were documented and are discussed within the description of the paleoseismic events. The fault F 1.1 is the most evident one (**Figs. 10C and 10D**). Faults F 1.1 and F2 are normal and F 1.2 and 3 are reverse. In other observed fractures, it is difficult to assign a magnitude of displacement, either because lower layers are apparently unaffected or because the stratigraphic contacts are highly irregular.

Laguna East trench

The Laguna East trench extends from the base of the scarp towards the lacustrine plane (**Fig. 4**). The trench was 47 m in length, 2-3 m in depth, and 2 m wide. In its southern part, this trench exposed a succession of three colluvial units (C1, C4-5) derived from the topographic scarp located to the south. The colluvial units are inter-layered with the Bañí ignimbrite and with lacustrine desposits towards the north. The ignimbrite is covered by brown sand deposits, showing cross-bedding and mostly composed of volcanic ash and small clasts of pumices and andesitic lavas. This deposit apparently resulted from reworking of loose ash, pumice and lithics from the non-welded top of Bañí ignimbrite. The lacustrine sequence consists of two silty units (FL 2-3) at the base of the trench and of a fine grained conglomerate, sand and

minor silt layers at the top of it (FL 1). In the central and northernmost parts of the trench, the ignimbrite overlies a brown paleosoil (S.2) and has a total thickness of about 1 m. Present-day soil (S.1) has been developed either on fine grained colluvial deposits of the footwall as on the sand and silt fluvial deposits of the hanging wall (**Fig. 7C, 7D** and **8**).

Three fault zones (F 4, F5 and F6) were identified along with two gentle folds affecting the lacustrine basal layers. The faults affect all the stratigraphic levels except the younger colluvium (C.1), the upper lacustrine unit (FL. 1) and the present-day soil developed on top of them. Gentle folding was observed in the lower silt layer (FL.3) in the northern part of the trench. Displacement of the stratigraphic layers was observed in three fault zones (F4, F5, and F6) and is discussed below. Single dip slip values observed in this trench range from 14 to 44 cm and are discussed in detail in the description of the paleoseismic events below. Fault Zone 4 corresponds to the main trace of the Pastores fault, striking N 80º - 94º E and dipping 65º - 68º to the N. In this fault zone, three fault planes are distinguishable on both walls of the excavation (F 4.1, 4.2, and 4.3). The faults displace the basal colluvial deposits and the ignimbrite. Several observations leads to recognize an increase in the fault thrown towards the east and a splay geometry of the fault array: **1)** Deformation of C.4 is greater on the eastern wall (**Fig. 7C**) than on the western wall (**Fig. 7D**); **2)** C.5 (or basal) unit is not exposed in the eastern wall, probably because it is affected by a greater down-thrown displacement; **3)** The distance between F 4.1 and F 4.2 is larger in the west wall. These horizontal branching, in scale, seems to correspond to the horse-tail splay of the main fault. Fault 4.1 is oriented N94ºE/65ºN and has slickenlines with a pitch of 85º/N indicating a minor right-lateral strike-slip component. In the colluvial levels affected by the fault F4.1, a large broken block aligned with the fault has slickenlines in agreement with the fault kinematics (pitch 86º/E within a pebble side oriented N80ºE/50ºN; **Fig. 8C**). Evidence of extensional deformation accommodated by this fault relies on an open fracture filled with material falling from the surface as can be seen in the E wall (**Fig. 8E**). Northwards, other faults and fractures filled by the ignimbrite (F 4.4 and F 4.5) suggest that the deformation was distributed in several structures with millimeter scale displacements. The Fault Zone 5 (F 5, **Fig. 7D**) is oriented N74ºE and it only affects the lower silt

layer (FL. 3). As F3, this fault is composed by multiple discontinuities characterized by tension fractures affecting the upper silt layer (FL. 2) and filled by the Bañí ignimbrite. At the southern part of this fault zone, gentle folding forming a monoclinal is affecting the upper silt layer (FL.2) and at the ignimbrite base (I.3), possibly associated with a north dipping blind inverse fault. The intermediate level of the ignimbrite (I.2) and upper layers appear undeformed by this fault zone. The Fault Zone 6 is oriented N62º-68ºE and displaces the lower (FL.3) and upper (FL.2) silt layers, and to lesser extent, the ignimbrite (F 6, **Fig. 7D**). In contrast to previously described faults, no tension fractures are present. This fault zone is apparently associated to folding in the silt layers, which produced two anticlines and a syncline in between. The ignimbrite unit fills the paleo-topography deformed by the folds.

Paleo-earthquake analysis of trenches at Laguna Bañí site

The analysis of the temporal relationship between the fault displacement and the deposition of the stratigraphic units was made following the criteria proposed by Villamor et al. (2011) for the study of paleoseismological trenches with presence/absence of tephra. The Bañí ignimbrite is a good stratigraphic marker to identify fault cutting relationships and it has permitted us to detect a minimum of 5 paleoseismic events caused by the slip along the northern WPF (**Table 2**). The 5 events are described below. The criteria used to attribute a co-seismic origin to the deformation observed are: **1)** displacement of a given unit cut by faults or folded, **2)** presence of open fractures sealed by overlying deposits, and **3)** geometry of the colluvial units controlled by fault related scarps in the paleo-surface.

Event 1- This is the youngest event and was identified by the stratigraphic discontinuity between the present-day soil level developed on top of colluvial unit C-1 and the ignimbrite. C1 fills a tension fracture of 26 cm of maximum aperture, observed only on the Laguna East trench E-wall (**Figs. 7C** and **8E**). This fracture is parallel to fault F 4.3. Neither the top nor the bottom of the ignimbrite seems vertically displaced along this fracture. Nearby joints affect the ignimbrite level (F 4.1 and F 4.2). Since the fracture is present only in one of the trench's walls and

given the cutting relationships, the deformation cannot be straightforward assigned to a seismic event in this fault. Most probably, the fracturing was produced as a secondary geological effect associated to the rupture of a different fault or fault segment, as it could be the central part of the Pastores fault or any other seismogenic fault in the area. A maximum age for this event of 990 – 1155 yrs AD was yielded by a sample of the soil filling the F 4.3 fracture (**Fig. 8E**). This age should be considered only indicative of the maximum age, since the colluvial material filling the fracture could have formed in a previous undetermined time before the opening of the coseismic fracture.

The Bañí site is at only at ~24 km from the 1912 earthquake epicenter and at 4 km to the west from the tip of the fault segment of the Pastores fault coseismic rupture, mapped by Urbina and Camacho (1913), and revisited by several authors (e.g.,Suter et al. 1995; Langridge et al. 2000: Rodríguez-Pascua et al., 2012). We suspect that co-seismic opening of fracture F 4.3 is contemporaneous to the 1912 Acambay earthquake; according to the testimony of the local inhabitants, a natural spring located next to the Laguna Bañí dried up during the 1912 Acambay earthquake and was never active again. We have interpreted this observation as a possible evidence of hydraulic alteration due to coseismic shacking, which would correspond to an intensity VIII-X in the Environmental Seismic Intensity (ESI) scale proposed by Michetti et al. (2007). For such intensity, the areas showing secondary earthquake effects range between 100 and 5000 km^2, so that the Bañí site is located within the expected area of affection.

Event 2- The second most recent event was inferred from the clear displacement of the base of the Bañí ignimbrite by several faults (F3, 4) and fold related faults (F5). This deformation, observed at both trenches, does not affect the upper part of the unit. In Laguna West trench, it can be observed how fault F3 displaced the base of the ignimbrite and the colluvial units underneath (C.2 and C.4). The offset is ~ 15 cm with an apparent vertical displacement to the south. Fault F 1.1 offsets the base of colluvial C.3 by 9 cm along dip and does not affect unit C.1. We know that event 2 is contemporaneous to the ignimbrite, so the time bracket for this displacement (between unit C.3 and C.1) is compatible with this earthquake as well as with the

previous one. . In Laguna East W-wall (**Fig. 7B**), fault F 4.5, material from the C.4 colluvial unit seems to be injected up into the ignimbrite. In Laguna East trench E-wall, faults F4.1 and F 4.3 displaced the base of the ignimbrite by 18 and 11 cm with an apparent dip displacement to the north, resulting in29 cm summed slip (maximum slip observed; **Fig. 7C**). The different displacements observed from one trench wall to the other suggest a lateral decrease towards the west in the fault displacement, which is also observed in the deformation caused in event 1. Event 2 should have occurred during the ignimbrite deposition (around 753 – 406 yrs BC), since only its base is affected. This fact can be explained if the paleo-earthquake occurred just after the deposition of the first phase in the eruptive activity that formed the ignimbrite.

Event 3- This event deformed all layers deposited before the Bañí ignimbrite and is associated with several unconformities and structural features including, **1)** open fractures developed in the layers beneath the ignimbrite; these fractures are observed at Laguna East W-wall and are coincident with faults F 4 (4.2, 4.3, 4.4), and they are filled up with ignimbrite material from I.1 in the southern area (**Fig. 7D**, **Fig 8B**); **2)** a fold observed at Fault Zone F 5 (**Fig 7D**); the lacustrine deposits FL 1 and 2 are folded; this folding implies a vertical apparent thrown to the south of 28 cm and it is sealed by the ignimbrite deposit; **3)** displacement along two fault zones (F1 and F 6.1); it was measured 9 cm of apparent dip displacement along F 1.1 (down to the north) and 7 cm of dip apparent displacement along F 6.1 (down to the south; **Figs. 9** and **10**). The maximum amount of displacement is 10 cm down to the south in Laguna East W-wall. This event took place after the deposition of colluvial units C.3 and C.2, after the formation of paleosoil deposit S2 (2134 – 1891 BC) and short before the ignimbrite emplacement; that is, before 753 – 406 yrs BC. The tension fractures were preserved with rectilinear geometries indicating a small elapsed time between their formation and the deposition of the ignimbrite, which acted as a sealing deposit.

Event 4- The analysis of the deformation affecting the basal colluvial deposits (base of C.4 and C.5) near the major fault scarp (Faults F 1, 2, and 4) allowed the identification of this event in the two trenches. The event also activated faults F 5 and 6, affecting the lacustrine basal units FL.2 and FL.3. In Laguna West trench, this

event caused deformation distributed in at least three fault branches, offsetting the top of unit C.4'' with 7 cm of dip displacement along F 1.1 (16 cm minus 9 produced in event 3 or 2), 20 cm of reverse displacement along F 1.2, and a total of 20 cm of dip displacement along F 2. On fault F 2, the deformation is accomplished by several faults resulting in the apparent "downthrown" injection of fragments of level C.4' into C.4''. This latter feature, also observed in F 4.5 during event 2, and the combination of apparent normal and reverse faulting are interpreted as resulting from local transpression, which might be occurring in particular fault bends (**Fig. 7A**). In Laguna East trench W-wall, fault F 4.1 cuts through the top of C.5 with 29 cm of apparent dip displacement, and displaces the basal part of C.4, but not the upper part. At a close view fault F 4.1 shows 29 cm of apparent dip displacement, but the surface envelope of C.5 practically does not show vertical offset. A plausible explanation for this inconsistency is the obliteration of the vertical component of slip by erosion along the slope; thus, the contact between C.5 and C.4 might be an erosive boundary implying a leveling of the paleosurface of the upthrown and downthrown blocks on both sides of F 4.1. Fault Zone 5 presents open fractures affecting the lacustrine deposits FL 2 and FL 3. These fractures are filled up with material from the paleosoil S2. It also affects these units causing discrete displacements (**Fig. 7D** and **Table 2**). At Fault Zone 6, a fold with associated faulting affects FL2 and FL3 and is sealed by paleosoil S2. Near 12 cm of apparent dip displacement (down to the south) is inferred in relation to the fold accommodation. This value is derived from 13 cm of reverse faulting at F 6.1, resulting from the 20 cm of down to the south minimum displacement of FL. 2 minus 7 cm added by event 3, and 25 cm of normal faulting at F. 6.2, which is the sum of 19 and 6 cm dip slip affecting FL. 2/FL1 contact. The total amount of displacement recorded in this event is 37 cm down to the north. This event occurred during the deposition of unit C 4' (between C3 and the base of C4'), as shown in Laguna West. At Laguna East, the event is constrained by FL2 and S2; it should have occurred right before or during the formation of paleosoil S2; Because S2 is filling some fresh fractures but it is not affected by the folds and faults, we infer thatit could be already present at the surface as a non-confined cover when the earthquake occurred. So, a preferred age for this even is that of paleosoil S2 at 2134 – 1891 yrs BC.

Event 5- An older event is inferred to be recorded in both trenches. The main evidence for this is derived from the geometry of the basal part of unit C.4. In Laguna West trench, the C.4" unit is only observed in the down-thrown block of fault F 2, which suggests that a topographic scarp had been formed prior the deposition of this unit. In Laguna East W-wall, the thickness of C.4 unit increases abruptly on top of F 4.3, which likely results from the filling of a topographic relief controlled by the fault activity. Evidence of displacement in this fault zone also comes from the fault striations preserved in a clast located along F 4.1. The striations have a pitch of 86ºE on a clast side oriented N92E, parallel to the fault zone (**Figs. 7A, 7D** and **8C).** In F 2, the faults are not coincident with the paleo-scarp but separated more than 2 m (F 2). This feature could be related to the scarp retreating linked to the erosive processes controlling the slope dynamics. There is evidence suggesting that this is a multiple event; on one hand, the exceptionally large displacements observed (compared to the displacement estimated for the posterior events) that are more easily explained by the sum of at least two consecutive events; the step on the paleo-surface sealed by C.4 near F 2 implies a downthrown offset of 85 cm, of which 20 cm are attributable to younger events. This yields 65 cm of dip displacement for the event 5 in F 2 (Laguna West E-wall, **Fig. 7A**). Fault F 4.3 apparently displaced the top of C.6 by 21 cm (laguna East W-wall, **Fig. 7B**). On the other hand, the large scarp retreat observed in fault F 2 (more than 2 m and only observed in this event) implies a large time lapse before deposition of C.4, allowing erosion to act. The age of this event is constrained by the deposition of colluvium C.4 and C.5. As with Event 4, paleosoil S2 is the only age bracket (upper boundary) for this possibly multiple-phase event, that is, 2134 – 1891 yrs BC.

Striation data and net slip rate

Slickenlines observed in the striated pebbles located along different fault planes and in the fault zone F 4.1 indicate that the slip in this fault zone is essentially dip slip. These striations have pitches between 50 and 86E in planes oriented N90-110E, which indicates a main NNE-SSW extension with a small dextral component. These data suggest that a local variation of the stress is being reflected in the Bañí

most recent events or that small rotation of the axis of extension with respect to the Pleistocene NW extension could have taken place in the late Holocene.

Another relevant structural observation refers to the varying total slip in the faults exposed in the trenches. Several faults show a throw opposite to the main fault; that is, down to the south instead of down to the north. As a result, the summed slip in one of the events (Event 3) results in 10 cm of throw towards the south (**Table 2**). It is likely that the faults with down-to-the-south thrown are antithetic faults. For this event we suspect that some other fault not exposed in the trenches, such as the southernmost branch of the splay, must be accommodating a larger thrown to north. Alternatively, the anomalous displacement could be due to the system acting as a a secondary structure related to an earthquake in a major neighboring fault. Transient and local variations of the stress regime produced by stress transfer after major earthquakes (e.g., Quigley et al., 2012) could also be evoked as an explanation of the reverse total throw.

In order to calculate the total amount of net displacement through the studied fault we considered an average 85ºE pitch for the main faults. This is the average pitch observed in Fault Zone 4, and in a striated pebble contained in it. The accumulated total vertical displacement calculated is 118 cm. This displacement initiated since the older colluvial unit (C.5) was formed. As we do not have an age for this colluvial unit, we estimated the maximum slip rate by considering the time span since the time of deposition of the paleosoil S2, (2134-1891 yrs BC) until present (1950 AD), which gives a maximum vertical slip rate of 0.29-0.30 mm/yrs. This value should be considered as a maximum, since the age of the marker considered is older than paleosoil S2. A rough estimate of the minimum vertical slip rate could be obtained by considering that the age of this older colluvial should not be more than 2,000 yrs, the age of the paleosoil S2. Such a long time span is sufficient for a soil to form in a setting such as the middle-late Holocene central Mexico, and also enough to ensure that there has not been a critical change in the environmental or depositional conditions of the site. Accordingly, the time span since 4134 – 3891 yrs BC leads to a minimum vertical slip rate of 0.19 -0.20 mm/yrs. We can estimate the net slip rate of this fault branch by calculating the net slip corresponding to a 60º dipping fault with

an 85º pitch, which results in 141 cm. Such a net slip accumulated along the same time spans gives a maximum net slip rate of 0.34-0.37 mm/yrs and a minimum net slip rate of 0.23-0.24 mm/yrs. These values of slip rate must be taken as approximate values since they are based on the deformation observed in only two fault branches and accumulated during the most recent 4 to 5 seismic events.

GPR SURVEY AT LAGUNA BAÑÍ SITE

Before trenching, the subsurface GPR prospection along four profiles allowed a more precise location of the faults in depth (**Figs. 5B and 9**). After trenching, the GPR results were improved with a detailed stratigraphic analysis in order to identify the deformation of a transect parallel to the trench, Ruedo 2 Profile, and located less than 10 m to the east (**Fig. 10**). Data and methods for GPR survey are explained in Appendix 1. **Figure 4** shows the location of the collected GPR profiles. During prospecting, a major vertical discontinuity interpreted as the main fault plane (LFB-4) was clearly recorded in the profile Ruedo 3 (**Fig. 9 E**). Similar discontinuities observed several meters north of the main fault plane were recognized in Ruedo 2 profile and were interpreted as secondary faults or fractures (**Fig. 10**). The main fault plane is clearly identified below the slope inflection in the topographic profile.

After trenching, stratigraphic units were sampled in order to measure its physical and mechanical properties. Samples of 2-3 kg were taken each 30 cm, along 2 vertical profiles in the trench Laguna East (**Figs. 4 and 7E**). These properties (**Table 3**) allowed assigning a value of permittivity to the GPR profiles. The contrast in physical properties helped in the identification of possible reflectors. Original profiles were filtered after comparison with the features observed in trenches Laguna East (near to Ruedo 2 profile) and Laguna West (directly below profile Ruedo 1). Profile Ruedo 3 was interpreted by interpolation of the before mentioned trenches and the field observations. An improved interpretation of the profiles (**Fig. 10**, discussed below) resulted from the comparison between GPR reflections and the materials described in trenches.

Interpretation of the deformation based on the comparison of GPR profiles and trench logs

We have detected a good agreement among radar signatures, coherent reflectors, and layers (sedimentary and volcanic) affected by faulting at the western termination of the Pastores Fault. The layers show variations of grain size and compaction. Electrical contrast between the inter-layered silty sand and ignimbrite allowed recording of coherent reflectors in GPR profiles. The fault branches were observed in the GPR profiles and the results can be compared directly with the Laguna East trench. The physical properties analyses in depth show a good correlation with the stratigraphy observed and with the radar signatures recorded. Once calibrated with the stratigraphy, textures and structures were recognized in radargrams allowing a better differentiation of units along the profile. **Figure 9** shows four GPR profiles and **Figure 10** the interpretation of the GPR reflections of Ruedo 2 profile. GPR profiles show a distribution of reflections similar to the stratigraphy observed at the trenches; that is, layers slightly dipping to the North in the footwall, interrupted reflectors in the zone of faulting, and subhorizontal reflectors in the hanging wall. Heterogeneity of the radar signature is observed in correspondence with the presence of fractures and possibly the presence of infiltrated water and/or higher clay content. The southern part of the profile is characterized by prominent reflectors related to pyroclastic deposits or high compaction of sediments.. GPR profiles also show evidence of what is interpreted as fault slip and fracturing in the hanging wall, suggesting that the deformation affects a wider zone than just the fault zones 1 to 4 (corresponding to topographic scarps), in agreement with the interpretation of a fault splay in this area.

Results show that the GPR technique can yield good results to characterize deformation in wide fault zones and allows to extrapolate the observations obtained in trenches in order to identify displacements in neighbor faults transects. The interpretation of the Ruedo 3 profile (**Fig. 9C**) was of particular importance to identify changes in the fault geometry with respect to the Ruedo 2 profile. In this profile the LFB-4 (Fault Zone 4) and the LFB-5 (Fault Zone 5) were recorded.

Although this profile is not coincident with any trench (it is at an approximate horizontal distance of 30 m from the East trench), it can be assumed that the main horizontal reflector corresponds to the well consolidated Bañí ignimbrite (I.1-I.3), showing a high physical contrast with the overlying colluvial deposits. Some of the vertical displacements recorded on this unit do not correspond with topographic variations that are mainly associated with the deformation of colluvial deposits. An overall vertical displacement of the Bañí ignimbrite can be estimated to be greater than 60 cm, from which 30 cm account for displacement by the Fault Zone 4 in two steps at 2.5 and 4 m from the beginning of the profile, and other 30 cm account for displacement of the Fault Zone 5 at a distance of 17 m from the beginning of the profile. At a distance of 30 m, another displacement of more than 20 cm corresponds to a fault branch that was not mapped in surface or in the trenches but was recorded in the GPR profile.

DISCUSSION

The WPF seismogenic activity

The lack of simultaneous activity among the fault branches studied and the absence of a characteristic slip have major implications on the fault behavior of the WPF. The analysis of the overall data suggests that not all fault branches exposed in the trenches are active in each of the seismic events. For instance, in the Laguna East W-wall, F 4.3 was not active after Event 3 and F 4.1 does not show deformation after event 4; in Laguna West, F 1 and F 2 were not active during Event 1 and 2. This aspect recalls the need to perform multi-trench analysis and to compare different fault chronologies when studying complex fault systems as the Pastores fault. In this study, only the two of the three branches of the northern WPF are surveyed. (**Fig. 5A** and **B**). Although the paleo-earthquake chronology might be well represented in only those two branches, this issue should be considered when analyzing the paleoseismic history of the complete WPF.

Another relevant observation concerning the seismic behavior of the faults studied is that it does not follow a characteristic slip pattern and that the deformation observed in a single fault branch highly varies from one event to another (**Table 2**). The non-characteristic slip has been observed in many fault systems worldwide. The highly variable slip along the Gowk Fault zone in two consecutive earthquakes in 1981 and 1998 is an example of observed non-characteristic slip in observed fault ruptures (Berberian et al., 2001). Other examples of this behavior have been reported in paleoseismological studies in several zones such as the San Andreas Fault (e.g.: Rockwell and Meltzner, 2008), faults in New Zealand (e.g.; Berryman and Beanland, 1991) or faults in Japan (e.g.; Maruyama et al., 2007). In the case of the Bañí site, two plausible explanations can account for this variability. On one hand, the fact that some of the movements observed might be secondary faulting related to earthquakes produced in neighboring faults. In the most recent morphogenic seismic event, the 1912 Acambay earthquake, it is possible that the studied fault zone has moved by seismic triggering as discussed above. This could also be happening in each or at least some of the earthquakes produced by the Venta de Bravo fault, located only 2.5 km to the south. On the other hand, even if the ruptures are primary, the fault zone might experience variable patterns of displacement as a consequence of the rupture of different fault fragments along the trace or in depth.

It is interesting to note that transfer fault zones are commonly considered as the end of seismogenic segments when defining individual seismic sources. However, even if the faults are not linked at the surface, they might be connected at depth and preserve an unlinked geometry on the earth surface over long time spans (Soliva et al., 2008). The connection at depth of the Pastores and the Venta de Bravo fault needs to be explored in order to properly evaluate the seismogenic activity recorded at the Bañí site. This hypothetical connection at depth would imply that both faults are part of a single fault system that could reach 80 km in length. The maximum expected seismic magnitude in this area would increase significantly if such a long fault is not segmented. Further research could put some light in this issue; for instance, obtaining subsurface data by means of seismic lines or magnetotelluric prospection.

Paleo-earthquake chronology and paleoseismic parameters

In order to evaluate the paleoearthquake chronology recorded at the Bañí site, we contemplate four possible models or combinations of the dating results (**Fig. 11**). Model A considers that the ignimbrite was deposited more recently, at some time between 753 - 406 BC, by giving as correct the age of sample C19 and taking as re-worked sample C05. Model B implies that the ignimbrite was deposited long before, at some time between 2134 and 1512 BC. In this case, sample C19 is considered as rejuvenated, possibly in relation of humic acid interaction during the edaphic processes. Two variants of models A and B are proposed by considering that 1) the opening of fracture F 4.3 is contemporaneous to the sample dated in the fracture infill (C3, 990 -1155 BC) and 2) that the fracture opened during the Acambay earthquake (12th November 1912). The paleoearthquake chronologies proposed are poorly constrained mainly owed to the limited number of ^{14}C samples, to the fact that these are concentrated in the ignimbrite and that some of them have not been considered representative of the unit in which they are found (**Table 1**).

Although all these chronologies are feasible, we prefer Model A.2 (recent ignimbrite and coseismic features during the 1912 Acambay earthquake) as the most probable one by several reasons; on one hand, it is more likely that the deposition of the ignimbrite had eroded one part of the geological record (that formed after paleosoil S2 representing ca. 1,000 years) than the opposite option, in which the processes postdating the ignimbrite (its edaphization and deposition of fluvial-lacustrine materials) would have taken place along ca. 2,500 years. On the other hand, we consider that the opening of fracture F 4.3 affects the uppermost layers, so that it is likely to have occurred during the last centuries. The local testimony reporting drainage alterations in the area during the Acambay earthquake reinforces this option. Considering Model A.2 and taking as a single seismic event (or crisis) the two earthquakes before and after the ignimbrite, we obtain a time span between consecutive earthquakes that ranges between 1.1 and 2.6 ka, giving an averaged recurrence time of 1.85 ka. This time span is much smaller than the obtained for the Acambay fault (~ 3.6 ka, Langridge et al., 2000) and the WPF eastern tip (10 – 15 ka; Langridge et al., 2013).

With respect to the Acambay fault, the WPF average recurrence obtained here could be smaller because the slip rate of the WPF fault is greater, but it could also be explained due to the alternating activity of the WPF as a primary and secondary fault. Concerning the eastern tip of the WPF, we considered that the fault chronology provided by Langridge et al. (2013) doesn't necessary have to be the complete chronology of the WPF. According to these authors, the lack of evidence of fractures that could be related to the 1912 event suggests that the Pastores fault did not move during this earthquake, and that the map performed by Urbina and Camacho (1913) included the trace of this fault due to a misinterpretation of the earthquake's effects. Since their paleoseismological study is located in a branch of the fault located in the middle of the slope (**Fig. 3**), we think it is likely that such a branch had not been active during some of the events on this fault, which will also explain the relative large recurrence period obtained at that site. Urbina and Camacho (1913) do not provide numerical estimations of the co-seismic displacement of the Pastores fault but do precise that the offsets are comparable to other ruptures produced by the earthquake, in this case having the uplifted block to the south. The possible activation of the WPF as a secondary fault or its activation by eventual volcanic eruptions is another obstacle to establish a recurrence time for the WPF, but it could also be taken as the opportunity to have a complete record of the morphogenetic ($M \geq 5$) earthquakes affecting the area. That is, the time span between successive earthquakes will not tell as much about the recurrence period of the Pastores fault but about the recurrence period of a damaging earthquake at a given point. This consideration is important when taking into account recurrence uncertainties in a risk analysis that considers all possible seismogenic sources affecting a site (Zúñiga et al., 2011).

Simultaneous activity of the Pastores and Acambay faults

Faulting along a complex fault zone involving neighboring faults and fault segments has been shown to be common in different tectonic settings, especially those occurring at extensional or transtensional regimes (e.g., Beanland et al., 1989; Berryman et al., 2008; Hauksson et al., 2011; Fletcher et al., 2014). Also in the Acambay graben and according to the descriptions of Urbina and Camacho (1913),

879 multiple faults ruptured during the Acambay earthquake. Comparing the
880 paleoearthquake chronologies of neighboring faults might help to evaluate the
881 feasibility of simultaneous ruptures (e.g., Berryman et al., 2008, Ortuño et al., 2012).
882 The precision of the dating results conditions the possibility to compare and identify
883 common earthquakes in different sites based on the age of the events. In this study,
884 the paleoearthquake chronology only allows us to consider that the simultaneous fault
885 rupture of the Acambay and the WPF is feasible based on the dating results, but does
886 not allow us to infer an unequivocal simultaneous behavior.

887 We have compared the data obtained here with the available neighboring fault
888 chronologies, the Acambay and Pastores faults, in order to put some light in this issue
889 (**Fig. 12**). Langridge et al. (2000) identified a minimum of 4 Holocene
890 paleoearthquakes recorded along the Acambay fault. In the eastern tip of the WPF at
891 Manto del Rio site, Langridge et al. (2013) recognized at least 3 paleoearthquakes
892 occurred in the last 31.5–41.0 cal ka BP, the most recent one constrained between
893 12.2 and 12.6 cal ka BP. The paleoseismic events identified at the Laguna Bañí site
894 (western tip of WPF) only reflect the most recent history of faulting in the area, that
895 is, the last 5-6 ka BP, and thus, they can only be compared with the paleoseismic data
896 at the Acambay fault. The five events identified at Bañí site occurred after 2134-1891
897 BC. The chronology proposed in model B.1 leads to consider that all the identified
898 paleoearthquakes could correspond to events on the Acambay fault; event 1 could be
899 the secondary effect during the 1912 earthquake; events 2, 3 and 4 could be
900 correlative of event 2 on the Acambay fault; multiple-event 5 could be event 3 on the
901 Acambay fault. In contrast, model A.1 implies that event 2 is not contemporaneous of
902 any event recorded in the Acambay fault. The close interaction between the
903 ignimbrite deposition and the activity at the western tip of the WPF, as evidenced by
904 stratigraphic relationships, can also be extrapolated to the Acambay fault, which
905 could have influenced the formation of the Bañí ignimbrite if model B.1 is the correct
906 one; in other words, Bañí ignimbrite emplacement could have been syn-tectonic with
907 faulting along the Acambay fault. The correlation between ignimbrites and
908 extensional faults has been observed in older ignimbrites of Mexico related with
909 Basin and Range faulting (Aguirre-Díaz and Labarthe-Hernández, 2003; Aguirre-
910 Díaz et al., 2008). For model A.1, the Bañí ignimbrite would not be related with any

paleoseismic event recorded in the Acambay fault, and alternatively, it could be under the influence of the major neighboring Venta de Bravo fault or just connected with the Pastores fault rupturing alone.

Other paleoseismic parameters

Besides the paleoearthquake chronology, other paleoseismic data such as slip per event, slip rate and maximum expected magnitude are commonly incorporated in the calculations of the seismic hazard. The maximum vertical slip per event experience at the Laguna Bañí ranges between 29 cm (Event 2) and 37 cm (Event 4, **Table 2**). As discussed above, summed slip in event 3 has been considered anomalous for being a reverse slip. The net slip per event is expected to be slightly greater. For a 60º average dip and 85º pitch, this would range between 35 cm and 44 cm. These values should be taken as minimum for the Pastores fault because 1) they refer to the tip of the fault, and 2) they do not reflect the slip accommodated in other fault branches along the same transect. These values of slip are in agreement with the displacements observed in the other paleoseismological sites within the region, such as the Manto del Rio site at the WPF eastern end (50 – 30 cm, Langridge et al., 2013), and the Huapango basin sites at the Acambay fault eastern end (~ 35 cm, Langridge et al., 2000). It is worth to note that all these sites are located at the tip of fault systems. If considered as representative of a minimum estimate of the average displacement, the 35 – 44 cm of slip per-event in Bañí site can be related to minimum moment magnitudes of 5.8 and 5.9 respectively according to Wells and Coppersmith (1994) relationship for normal faults. We recommend taking these values just as rough estimations, being aware that the empirical relationships used have being questioned in the last decade (Stirling et al., 2002; 2013).

Another approach to the maximum expected magnitude can be done by taking into account the WPF total length, 20.4 km. Using the Wesnousky (2008) scaling relationships recommended by Stirling et al (2013) for normal faults within settings of crust thicker than 10 km, the obtained moment magnitude is 6.7. The crustal thickness in the region is likely to range between 12 and 20 km, based on the highest

941 densitieshighest accumulation of seismicity of hypocentral depths at that depth of the
942 seismic for crustal events published recorded by the Mexican Seismological Survey
943 (SSN).

944 The dating results and displacements observed at the trenches indicate
945 minimum estimates for the WPF slip rates in the range of 0.23 – 0.37 mm/yr for the
946 last ~6-4 ka. These values for slip rates are much larger than the values obtained by
947 Langridge et al. (2000) for the Acambay fault, estimated at 0.17 mm/yr and overpass
948 the 0.17 - 0.18 mm/yr maximum vertical slip rates for the Quaternary faults in the
949 Central TMVB estimated by Suter et al. (2001). Other slip rates obtained for the
950 Pastores fault are 0.03 mm/yr since ~ 10 ka ago, given by Langridge et al. (2013) for
951 the eastern tip of the WPF and 0.04 mm/yr since ~ 400 ka ago given by Suter et al.
952 (1995) for the western tip of the EPF. In our opinion, both estimated slip rates should
953 be considered as minimum values, the former, at 0.03 mm/yr, considers only a branch
954 of this fault located at the middle of the WPF scarp; the latter, at 0.04 mm/yr, is a
955 rough estimate since, according to Suter et al. (1995), the slip considered is not clear.
956 One should be cautious when comparing slip rates at paleoseismological sites with
957 geological slip rates. Most of the published slip rates of the Central TMVB are
958 calculated considering Middle to Early Pleistocene volcanic markers and minimum
959 throws, since they are based on the height of the topographic scarps but do not
960 consider that the marker might be at a much lower position in the downthrown block,
961 covered by most recent deposits. For instance, the Bañí transect, a geological slip rate
962 of 0.02 mm/yr is obtained using 85 m of scarp height accumulated in 3.5 Ma, which
963 is the most probable age of the lavas located to the SSW based on their comparison
964 with the similar intracaldera domes within the Amealco caldera and within Puruagua
965 range (**Fig. 3**; Aguirre-Díaz, 1996).

966 Other estimates of slip rates for the Central TMVB faults were given by Ego
967 and Ansam (2002). These authors obtained vertical slip rates of 3 mm/yr for this area
968 by considering the 0.8 cm/yr theoretical arc-parallel rate of the Middle American
969 Trench. It is difficult to test if the estimates of these authors are realistic, because the
970 number of active structures within the area is unknown. Suter et al. (2001) estimate in
971 5 to 10 the number of faults that show Quaternary activity within a 30 -50 km cross

section of the Central TMVB, which according to the summed vertical rates given by Ego and Ansam (2002) results in minimum 0.3 mm/yr vertical slip rates for individual faults, being this value in agreement with our results.

Even if our slip rate estimate is based on limited field observations and could be overestimated, we believe that the slip rates in the Acambay graben should be revised in order to obtain realistic Holocene rates, which would be more relevant for the seismic hazard calculations than the geologic rates. Could the WPF Holocene slip rate be larger than the geological slip rate, thus indicating a late Quaternary acceleration of the fault rate? Is the WPF westernmost tip moving faster as a consequence of the linkage at depth of the Pastores and Venta de Bravo faults, which would make this site to be located in middle rather than a marginal fault segment? These questions stay unresolved and could lead future research.

Paleoearthquake chronology and volcanic activity

Two age results were obtained for Bañí ignimbrite, 753 – 406 yrs BC and 2,196 – 1,512 yrs BC, being the former the preferred age. Even if considering both dates, the recent age of the Bañí ignimbrite obtained in this study contrasts with all the former ages for late Quaternary volcanic deposits obtained in the Acambay graben, with the exception of two other ignimbrites (Ortuño et al., 2011; Aguirre-Díaz et al., 2012; Lacan et al., 2013) and a tephra deposit (Langridge et al., 2013); all of them exposed in nearby paleoseismological trenches (**Fig. 3**). The trenches exposures indicate that two of the seismic events occurred just prior to the ignimbrite emplacement (Event 3) and right after it (Event 2). This suggests that seismic Event 2 was likely triggered by volcanic activity and/or that seismic event 3 triggered the pyroclastic flow. As mentioned above, similar relationships between pyroclastic flow eruptions and extensional tectonics has been reported in ignimbrites of mid-Tertiary Sierra Madre Occidental of Mexico (Aguirre-Díaz and Labarthe-Hernández, 2003; Aguirre-Díaz et al., 2008). The interaction between volcanic and tectonic activity has been detected and analyzed in different geodynamical scenarios worldwide (e.g., Gottsmann et al., 2009, Petrinovic et al., 2010, Villamor et al., 2011). In the Laguna

Bañí, the interaction between the ignimbrite emplacement and the fault activity might be the reflection of seismogenic activity advanced by a change in local stress field as a result of volcanic activity, thus implying subsurface magmatic processes, probably related with activity of the nearby Altamirano stratovolcano (**Fig. 3**). This could explain the short time span between Events 2 and 3. Additionally, the occurrence of Event 3 could have caused a change in the magma chamber stress conditions leading to the ignimbrite-forming eruption. An alternative scenario can be envisaged considering that no subsurface volcanic changes are needed to occur right before the formation of the ignimbrite, but only the previous generation of a dome at surface whose explosive eruption is triggered by seismic amplification. To discern among the different possible scenarios, more regional data on the temporal and spatial relationship between volcanism and seismic activity is needed, as well as a better knowledge of the source and emplacement mechanisms of Bañí ignimbrite. The volcanic-tectonic interaction within the Acambay graben is a promising and unexplored research field that has a great impact in the evaluation of the seismic recurrence interval obtained in the paleoseismological studies in the region. Additionally, the volcanic hazard in the area, which nowadays is considered very low, should be revised for a better evaluation of the volcanic risk in this part of the Transmexican Volcanic Belt (Aguirre-Díaz et al., 2012, 2013).

CONCLUSIONS

The following conclusions can be drawn from the study presented here:

1) The geomorphological and structural study, combined with geologic mapping allowed to re-define the surface trace of the Western Pastores fault, which has a total 20.4 km length and a westernmost tip composed of two fault branches. Two paleosesimic trenches were excavated in the northernmost branch of this tip, where the fault movement has generated a sag pond, where Laguna Bañí was formed. GPR prospecting of the area combined with the detailed study of the sequences led to an appropriate location of the subsurface faults before trenching and the estimation of the average vertical displacements in the two recorded fault

branches (LFZ-4 and LFZ-5). After the excavation, characterization of samples improved radar processing as the variations of physical properties of several reflectors permitted the identification of increasing-to-the-east offsets in stratigraphic markers along non-trenched sections. High physical contrasts between the prospected sequences, such as variations in grain size distribution or between colluvial and well consolidated pyroclastic deposits, can be of great help to improve assessment of local slip rates.

2) The stratigraphic and structural analysis of the sequence at the Laguna Bañí site led us to identify a colluvial-volcanic and fluvio-lacustrine sequence affected by complex faulting that implies discrete displacements in synthetic and antithetic faults oriented ~ E-W. We confirm late Holocene volcanic activity within the Acambay graben, which alerts about the need of a re-evaluation of the local volcanic hazard.

3) The Bañí sequence records at least five paleoearthquakes: Event 1 occurring after 990 -1155 AD and most probably during the 1912 Acambay earthquake; Event 2 during the preferred time span 753 - 406 BC; Event 3 and Event 4 shortly after and before the emplacement of an ignimbrite at an age bracket of 2134-1512 BC; and Event 5 (multiple event) at some undetermined time before the ignimbrite.

4) Different faults zones within the WPF were activated at each of the paleoearthquakes identified. This and the highly variable slip per event observed suggest that the northern WPF could move occasionally as a secondary fault of major neighboring structures such as the Acambay and Venta de Bravo faults. This idea is supported by the anomalously small time span between the successive events (1.1-2.6 ka).

5) The studied site shows that neighboring volcanic activity is likely to have been a triggering factor and/or a consequence of the seismogenic activity. The time association of volcanic and tectonic events indicates that such interaction must be taken into account when obtaining recurrence periods from the paleoseismological record and recalls the need of an integrated database of volcanic and paleoseismic results for this region.

ACKNOWLEDGEMENTS

This research was founded by UNAM Program for Research and Technological Innovation (PAPIIT) Grant IN112110 and by the National Council of Science and Technology–Mexico (CONACyT) Grant CB-2009-01-129010. The geomechanical analysis were done by Ricardo Carrizosa Elizondo at the Laboratorio de Mecanica de Geosistemas (LAMG) of Centro de Geociencias UNAM at Queretaro City. We are thankful to Celine, Simon, Avith, Neto, Estefania, Rosanna, Angel and Rosa María for the field assistance and to the landlords of the paeloseismological site, Antonio and Alfonso Camacho-Saldivar.

REFERENCES CITED

Aguirre-Díaz, G.J., 1995, La Toba de Amealco y su correlación con la Formación Las Américas a través del graben de Acambay, parte central de la Faja Volcánica Mexicana: Revista Mexicana de Ciencias Geológicas, v. 12, p. 17-21.

Aguirre-Díaz, G. J., 1996, Volcanic stratigraphy of the Amealco caldera and vicinity, Central Mexican Volcanic Belt: Revista Mexicana de Ciencias Geologicas, v. 13, p. 10-51.

Aguirre-Díaz, G.J., and Labarthe-Hernández, G., 2003, Fissure ignimbrites: Fissure-source origin for voluminous ignimbrites of the Sierra Madre Occidental and its relationship with Basin and Range faulting: Geology, v. 31, p. 773-776.

Aguirre-Díaz, G.J., and McDowell, F.W., 2000, Volcanic evolution of the Amealco caldera, central Mexico: *in*: Delgado-Granados, H., Stock, J., Aguirre-Díaz, G.J., (eds.), Cenozoic Tectonics and Volcanism of Mexico, Boulder, Colorado, Geological Society of America Special Paper 334, p. 167-178.

Aguirre-Díaz, G.J., Ferrari, L., Nelson, S.A., Carrasco-Núñez, G., López-Martínez, M., Urrutia-Fucugauchi, J., 1998, El Cinturón Volcánico Mexicano: Un nuevo proyecto multidisciplinario: Unión Geofísica Mexicana, Geos, v. 18, p. 131-138.

Aguirre-Díaz, G.J., Labarthe-Hernández, G., Tristán-González, M., Nieto-Obregón, J., Gutiérrez-Palomares, I., 2008, Ignimbrite Flare-up and graben-calderas of the Sierra Madre Occidental, Mexico: *in* Gottsmann, J. and Martí, J. (eds.), Caldera Volcanism: Analysis, Modelling and Response, Developments in Volcanology 10, Elsevier, Amsterdam, 492 p., (143-180 pp.), ISBN 978-0-444-53165-0.

Aguirre-Díaz, G.J, Nieto-Obregón, J., Zúñiga, R., 2005, Seismogenic Basin and Range and intra-arc normal faulting in the central Mexican Volcanic Belt,

Querétaro, México: Geological Journal, v. 40, p. 1-29.
Aguirre-Díaz, G., Ortuño, M., Zúñiga, R., Lacan, P., Persaud, M., 2012, Late Pleistocene-Holocene explosive volcanism in the Acambay graben: A change to the status of this zone of central Mexico to one of potential volcanic danger: Cities on Volcanoes, Colima, 19-23 November, International Association of Vulcanology and Chemistry of the Earth's Interior.
Aguirre-Díaz, G.J., Ortuño, M., Lacan, P., Zúñiga, R., Roldán-Quintana, J., Suñe-Puchol, I., Audin, L., Baize, S., Persaud, M., Lawton, T., 2013, Recent volcanic activity in the Acambay graben: Reunión Anual Unión Geofísica Mexicana 2013, Geos, v. 33, No. 1.
Aguirre-Díaz, G.J., Urrutia-Fucugauchi, J., Soler-Arechalde, A.M., McDowell, F.W., 2000, Stratigraphy, K-Ar ages, and magnetostratigraphy of the Acambay graben, central Mexican Volcanic Belt: *in* Delgado-Granados, H., Aguirre-Díaz, G., Stock, J.M. (eds.), Cenozoic Tectonics and Volcanism of Mexico, Boulder Colorado, Geological Society of America, Special Paper 334, p. 167-178.
Alaniz-Alvarez, S. A., y Nieto-Samaniego, A.F, 2005, El sistema de fallas Taxco-San Miguel de Allende y la Faja Volcánica Transmexicana, dos fronteras tectónicas del centro de México activas durante el Cenozoico: Boletín de la Sociedad Geológica Mexicana, vol. 42, p. 65-82.
ASTM D6913-09, 2009, Standard test methods for particle-size distribution (gradation) of soils using sieve analysis: American Society for Testing and Materials.
ASTM D854-10, 2010, Standard test methods for specific gravity of soil solids by water pycnometer: American Society for Testing and Materials.
ASTM D4318-10, 2010, Standard test methods for liquid limit, plastic limit, and plasticity index of soils: American Society for Testing and Materials.
ASTM D2487-11, 2011, Standard practice for classification of soils for engineering purposes (Unified Soil Classification System): American Society for Testing and Materials.
Bahat, D., 1981, Certain mechanical aspects in comparative continental rifting with a special reference to the Baikal rift: Geological Magazine, v. 118, p. 271-280.
Beanland, S., Berryman, K.R., Blick, G.H., 1989, Geological investigations of the 1987 Edgecumbe earthquake, New Zealand: New Zealand Journal of Geology and Geophysics, v. 32:1, p. 73-91.
Berberian, M., Jackson, J. A, Fielding, E., Parsons, B. E., Priestley, K. and Qorashi, M., 2001, The 1998 march 14 Fandoqa earthquake (M_w 6.6) in Kerman province, Southeast Iran: re-rupture of the 1981 Sirch earthquake fault, triggering of slip on adjacent thrusts and the active tectonics of the Gowk fault zone. Issue. Geophysical Journal International. v. 146: 2, p. 371–398. DOI: 10.1046/j.1365-246x.2001.01459.x.
Berryman, K., and Beanland, S. , 1991, Variation in fault behaviour in different tectonic provinces of New Zealand. Journal of Structural Geology, v.13: 2, p.

177–189. DOI: 10.1016/0191-8141(91)90065-Q
Berryman, K., Villamor, P., Nairn, I., van Dissen, R., Begg, J., Lee, J., 2008, Late Pleistocene surface rupture history of the Paeroa Fault, Taupo Rift, New Zealand: New Zealand Journal of Geology and Geophysics, v. 51:2, p. 135-158.
Carbonel, D., Gutierrez, F., Linares, R., Roqué, C., Zarroca, M., McCalpin, J., Guerrero, J., Rodriguez, V., 2013, Differentiating between gravitational and tectonic faults by means of geomorphological mapping, trenching and geophysical surveys. The case of the Zenzano Fault (Iberian Chain, N Spain): Geomorphology, v. 189, p. 93-108.
Carreón-Freyre, D. C., Cerca, M., Hernandéz-Marín, M., 2003, Correlation of near-surface stratigraphy and physical properties of clayey sediments from Chalco Basin, Mexico, using Ground Penetrating Radar: Journal of Applied Geophysics, v. 53, p. 121-136.
Carreón-Freyre, D., and Cerca, M., 2006, Delineating the near-surface geometry of the fracture system affecting the valley of Queretaro, Mexico: Correlation of GPR signatures and physical properties of sediments: Near Surface Geophysics, EAGE (European Assoc. of Geoscientists and Engineers), v. 4(1), p. 49-55.
Comas, X., Slater, L., Reeve. A., 2005, Spatial variability in biogenic gas accumulations in peat soils is revealed by ground penetrating radar (GPR): Geophisical Research Letters, v. 32, p. 1-4.
Cunningham, K.L., 2004, Application of ground-penetrating radar, digital optical borehole images, and cores for characterization of porosity hydraulic conductivity and paleokarst in the Biscayne aquifer, southeastern Florida, USA: Journal of Applied Geophysics, v. 55, p. 61-76.
Davis, J.L., and Annan, A.P., 1989, Ground penetrating radar for high resolution mapping of soil and rock stratigraphy: Geophysical Prospecting, v. 37, p. 531-551.
De Cserna, Z., 1989, An outline of the geology of Mexico: *in* Bally, A.W. and Palmer, A.R. (eds.), The Geology of North America – An Overview, The Geology of North America, Geological Society of America, Boulder, Colorado, v. A, p. 233-264.
Demant, A., 1978, Características del Eje Neovolcánico Transmexicano y sus problemas de interpretación: Instituto de Geología, UNAM. Revista Mexicana de Ciencias Geológicas, v. 2, p. 172-187.
Doolittle, J. A., and Collins, M. E., 1995, Use of soil information to determine application of Ground Penetrating Radar: Journal of Applied Geophysics, v. 33(1-3), p. 101-108.
Ego, F., and Ansan, V., 2002, Why is the Central Trans-Mexican Volcanic Belt (102° 99°W) in transtensive deformation? Tectonophysics, v. 359, p. 189-208.
Fam, M. A., and Santamarina, J. C., 1997, A study of consolidation using mechanical and electromagnetic waves: Geotechnique, v. 47(2), p. 203-219.
Ferrari, L., Orozco-Esquivel, T., Manea, V., Manea, M., 2012, The dynamic history

of the Trans-Mexican Volcanic Belt and the Mexico subduction zone: Tectonophysics, v. 522-523, p. 122-149.

Ferrill, D.A., Stamatakos, J.A., Sims, D., 1999, Normal fault corrugation: implications for growth and seismicity of active normal faults: Journal of Structural Geology, v. 21, p. 1027–1038.

Figueroa, J., 1970, Catálogo de Sismos ocurridos en la República Mexicana: Instituto de Ingeniería, UNAM, Reporte Interno No. 272.

Fletcher, J., Teran, O., Rockwell, T. K. , Oskin, M.E., Hudnut, K.W., Mueller, K.J., Spelz, R.M., Akciz, S.O., Masana, E., Faneros, G., Fielding, E.J., Leprince, S., Morelan, A.E., Stock, J., Lynch, D.K., Elliott, A.J., Gold, P., Liu-Zeng, J., González-Ortega, A., Hinojosa-Corona, A., González-García, J., 2014, Assembly of a large earthquake from a complex fault system: Surface rupture kinematics of the 4 April 2010 El Mayor–Cucapah (Mexico) Mw 7.2 earthquake. Geosphere, v. 10:4, p. 797-827.

García-Acosta, V., and Suárez, G., 1996. Los Sismos en la Historia de México, Tomo I. UNAM/CIESAS/Fondo de Cultura Económica, Mexico City, 719 p.

García-Palomo, A., Macías, J. L., Arce, J. L., Capra, L., Espíndola, J. M., Garduño-Monroy, V. H., 2000, Geology of Nevado de Toluca Volcano and surrounding areas, central Mexico: Geological Society of America Map Chart Ser., MCH099, 14 p.

Garduño-Monroy, V. H., Pérez-Lopez, R., Israde-Alcantara, I., Rodríguez-Pascua, M. A., Szynkaruk, E., Hernández-Madrigal, V. M., García-Zepeda, M. L., Corona-Chávez, P., Ostroumov, M., Medina-Vega, V. H., García-Estrada, G., Carranza, O., Lopez-Granados, E., Mora-Chaparro, J. C., 2009, Paleoseismology of the southwestern Morelia-Acambay fault system, central Mexico: Geofísica Internacional, v. 48 (3), p. 319-335.

Gómez-Tuena, A., Orozco-Esquivel, M. T., Ferrari, L., 2005, Petrogénesis ígnea de la Faja Volcánica Transmexicana: Boletín de la Sociedad Geológica Mexicana, Volumen Conmemorativo, Tomo LVII, 3, p. 227-283.

Gottsmann, J., Lavallée, Y., Martí, J., Aguirre-Díaz, G.J., 2009, Magma–tectonic interaction and the eruption of silicic batholiths: Earth and Planetary Science Letters, v. 284, p. 426-434.

Guha, S., Kruse, S.E., Wright, E. E., Kruse, U. E., 2005, Spectral analysis of ground penetrating radar response to thin sedimentary layers: Geology Faculty Publications Paper **7**.

Hauksson, E., Stock, J., Hutton, K., Yang, W., Vidal-Villegas, J.A., Kanamori, H., 2011, The 2010 Mw 7.2 El Mayor-Cucapah Earthquake Sequence, Baja California, Mexico and Southernmost California, USA: Active seismotectonics along the Mexican Pacific Margin: Pure and Applied Geophysics, v. 168 (8-9), p. 1255-1277.

Husker, A., and Davis, P. M., 2009, Tomography and thermal state of the Cocos plate subduction beneath Mexico City: Journal of Geophysical Research, v. 114,

1226 B04306.
1227 Johnson, C. A., and Harrison, C. G. A., 1989, Tectonics and volcanism in central
1228 Mexico: A Lansat Thematic Mapper perspective: Remote Sensing of
1229 Environment, v. 28, p. 273-286.
1230 Johnson, C.A., and Harrison, C.G.A., 1990, Neotectonics in central Mexico: Physics
1231 of the Earth and Planetary Interiors, v. 64, p. 187-210.
1232 Joyner, W. B., and Fumal, T. E., 1985, Predictive mapping of earthquake ground
1233 motion: *in* Evaluating Earthquake Hazards in the Los Angeles Region: An Earth
1234 Science Perspective, U.S. Geological Survey Professional Paper 1360, p. 203-
1235 220.
1236 King, G.C.P. Stein, R. S., Lin, J., 1994, Static stress changes and the triggering of
1237 earthquakes. Bulletin of the Seismological Society of America, v. 84:3, p. 935-
1238 953.
1239 Lacan, P., Zúñiga, F. R., Ortuño, M., Persaud, M., Aguirre-Díaz, G.J., Langridge, R.
1240 M., Villamor, P., Perea, H., Štěpančíková, P., Carreón, D., Cerca, M., Suñe
1241 Puchol, I., Corominas, O., Audin, L., Baize, S. Lawton, T. F., Rendón A., 2013,
1242 Paleoseismological History of the Acambay Graben (Central Mexico):
1243 Proceedings of the AGU Fall Meeting at San Francisco CA, Eos, v. 94, T23C-
1244 2591.
1245 Langridge, R., Weldon, R., Moya, J., Suárez, G., 2000, Paleoseismology of the 1912
1246 Acambay earthquake and the Acambay-Tixmadejé fault, Trans-Mexican
1247 Volcanic Belt: Journal of Geophysical Research, v. 105, p. 3019–3037.
1248 Langridge, R.M., Persaud, M., Zúñiga, F.R., Aguirre-Díaz, G. J., Villamor, P.,
1249 Lacan, P., 2013, Preliminary paleoseismic results from the Pastores fault and its
1250 role in the seismic hazard of the Acambay graben, Trans-Mexican Volcanic Belt,
1251 Mexico*: Revista Mexicana de Ciencias Geológicas*, v. 30, p. 463-481.
1252 León-Soto, G., Ni, J.F., Grand, S.P., Sandvol, E., Valenzuela, R.W., Speziale, M.G.,
1253 González, J.M.G., Reyes, T.D., 2009, Mantle flow in the Rivera–Cocos
1254 subduction zone: Geophysical Journal International, v. 179, 1004–1012.
1255 Martínez Reyes, J., and Nieto-Samaniego, A.F., 1990, Efectos geológicos de la
1256 tectónica reciente en la parte central de México: Revista Instituto de Geología, v.
1257 9, p. 33–50.
1258 Maruyama, T., Iemura, K., Azuma, T., Yoshioka, T., Sato, M., Miyawaki, R., 2007,
1259 Paleoseismological evidence for non-characteristic behavior of surface rupture
1260 associated with the 2004 Mid-Niigata Prefecture earthquake, central Japan.
1261 Tectonophysics, v. 429:1–2, p. 45–60. DOI: 10.1016/j.tecto.2006.09.008
1262
1263 Masana, E., Villamarın, J.A., and Santanach, P., 2001, Paleoseismic results from
1264 multiple trenching analyses along a silent fault: The El Camp fault (Tarragona,
1265 northeastern Iberian Peninsula): Acta Geológia Hispanica, v. 36, p. 329–354.
1266 McCalpin, J. P. (ed.), 2009, Paleosesmology, 2nd Edition: Academic Press-Elsevier,
1267 Amsterdam, 848 p.

McClymont, A., Green, A., Kaiser, A., Horstmeyer, H., Landgridge, R., 2010, Shallow fault segmentation of the Alpine fault zone, New Zealand, revealed from 2- and – GPR surveying: Journal of Applied Geophysics, v. 70, p. 343-354.

Meghraoui, M., Camelbeeck, T., Vanneste, K., Brondeel, M., Jongmans, D., 2000, Active faulting and paleoseismology along the Bree Fault Zone, Lower Rhine Graben (Belgium): Journal of Geophysical Research, v. 105, p. 13809-13841.

Michetti, AM., Audemard, F., Azuma, T., Clague, J., Comerci, V., Esposito E., Guerrieri, A., Gürpinar, A., McCalpin, J., Mohammadioun, B., Morner, NA., Ota, Y., Porfido, S., Roghozin, E., Serva, L., Tatevossian, R., Vittori, E., 2007, Intensity Scale ESI-2007; Memorie Descriptive Della Carta Geologica D'Italia, 74. APAT, SystemCart Srl, Roma, Italia.

Neal, A., 2004, Ground-penetrating radar and its use in sedimentology: Principles, problems and progress: Earth-Science Reviews, v. 66, p. 261–330.

Nieto-Samaniego, A., Ferrari, L., Alaniz-Álvarez, S., Labarthe-Hernández, G., Rosas-Elguera, J., 1999, Variation of Cenozoic extension and volcanism across the southern Sierra Madre Occidental Volcanic Province, Mexico: Geological Society of America Bulletin, v. 111, p. 347–363.

Nixon, G.T., 1982, The relationship between Quaternary volcanism in central Mexico and the seismicity and structure of subducted ocean lithosphere: Geological Society of America Bullettin, v. 93, p. 514-523.

Norini, G., Groppelli, G., Lagmay, A.M.F., Capra, L., 2006, Recent left-oblique slip faulting in the central eastern Trans-Mexican Volcanic Belt: Seismic hazard and geodynamic implications: Tectonics, 25, TC4012.

Ohtsubo, M., Takayama, M., Egashira, K., 1983, Relationships of consistency limits and activity to some physical and chemical properties of Ariake marine clays: Soils and Foundations, v. 23 (1), p. 38-46.

Orozco, E., and Berra, J.D., 1887, Efemérides seismicas mexicanas: Memorias Sociedad Científica ''Antonio Alzate'' (México), v. 1, p. 303–541.

Ortuño, M., Zúñiga, R., Corominas, O., Perea, H., Ramírez-Herrera, M.T., Štepancíková, T., Villamor, P., Aguirre-Díaz, G. J., Norini, G., 2011, Caracterización de fallas sismogenéticas en el centro del Cinturón Volcánico Trans–Mexicano. Resultados Preliminares: Book of abstracts of the XIV Latinoamerican Conference of Geology, Medellín, Colombia, p. 165-166.

Ortuño, M., Masana, E., García Meléndez, E., Martínez-Díaz, J., Štěpančíková, P., Cunha, P.P., Sohbati, R., Canora, C., Buylaert, J.P., Murria, A.S., 2012, An exceptionally long paleoseismic record of a slow-moving fault: The Alhama de Murcia fault (Eastern Betic Shear Zone, Spain): Bulletin of the Geological Society of America, v. 124 (9-10), p. 1474–1494.

Ovando-Shelley, E., Lermo-Samaniego, J., Auvinet, G., Méndez-Sánchez, E., 2012, Microtremor measurements to identify zones of potential fissuring in the basin of Mexico: Geofísica Internacional, v. 51-2, p. 143-156.

Pardo, M., and Suárez, G., 1995, Shape of the subducted Rivera and Cocos plate in

1310 southern Mexico: seismic and tectonic implications: Journal of Geophysical
1311 Research, v. 100, p. 12357–12373.
1312 Pasquaré, G., Vezzoli, L., Zanchi, A., 1987, Morphological and structural model of
1313 Mexican Volcanic Belt: Geofisica International, v. 26, p. 159 – 176.
1314 Pauselli, C., Federico, C., Frigeri, A., Orosei, R., Barchi, M., Basile, G., 2010,
1315 Ground penetrating radar investigations to study active faults in the Noarcia
1316 Basin (central Italy): Journal or Applied Geophysics, v. 72, p. 39-45.
1317 Pérez-Campos, X., Kim, Y., Husker, A., Davis, P.M., Clayton, R.W., Iglesias, A.,
1318 Pacheco, J.F., Singh, S.K., Manea, V.C., Gurnis, M., 2008, Horizontal
1319 subduction and truncation of the Cocos Plate beneath central Mexico:
1320 Geophysical Research Letters, v. 35, L18303.
1321 Persaud, M., Zúñiga, F.R., Aguirre-Díaz, G.J., Villamor, P., Langridge, R., 2006,
1322 First steps towards the paleoseismological history of the Pastores and Venta de
1323 Bravo Faults, Acambay Graben, Trans-Mexican Volcanic Belt, Central Mexico:
1324 Transactions of the American Geophysical Union, Fall Meeting, Eos, abstract
1325 T13B-0501.
1326 Petrinovic, I., Martí, J., Aguirre-Díaz, G.J., Guzmán, S., Geyer, A., Salado-Paz, N.,
1327 2010, The Cerro Aguas Calientes caldera, NW Argentina: an example of a
1328 tectonically controlled, polygenetic, collapse caldera, and its regional
1329 significance: Journal of Volcanology and Geothermal Research, v. 194 (1-3), p.
1330 15–26.
1331 Quigley, M., Van Dissen, R., Litchfi eld, N., Villamor, P., Duffy, B., Barrell, D.,
1332 Furlong, K., Stahl, T., Bilderback, E., Noble, D., 2012, Surface rupture during
1333 the 2010 Mw 7.1 Darfield (Canterbury) earthquake: Implications for fault rupture
1334 dynamics and seismic-hazard analysis: Geology, v. 40(1), p. 55-58.
1335 Ramírez-Herrera, M.T., Summerfield, M.A., Ortiz-Pérez, M. A., 1994, Tectonic
1336 geomorphology of the Acambay graben, Mexican Volcanic Belt: Zeitschrift fur
1337 Geomorphologie NF, v. 38, p. 151-168.
1338 Ramírez-Herrera, M. T, 1998, Geomorphic assessment of active tectonics in the
1339 Acambay graben, Mexican volcanic belt: Earth Surface Processes and
1340 Landforms, v. 23, p. 317 – 332.
1341 Rockwell, T. K., and Meltzner, A. J., 2008, Non-characteristic Slip and Earthquake
1342 Clustering on the Imperial Fault, Mesquite Basin, Imperial Valley, California.
1343 American Geophysical Union, Fall Meeting 2008, abstract #T11A-1845.
1344 Rodríguez-Pascua, M.A., Garduño-Monroy, V.H., Isdrade-Alcántara, I., 2004,
1345 Registros sísmicos purépechas del periodo preclásico (3,000 años), deducidos
1346 mediante la paleosismicidad. Isla de Jarácuaro, Lago de Páztcuaro, Michoacán,
1347 México: Geo-Temas, v. 6(3), p. 191-194.
1348 Rodríguez-Pascua, M.A., Garduño-Monroy, V.H., Israde-Alcántara, I. & Pérez-
1349 López, R., 2010, Estimation of the paleoepicentral area from the spatial gradient
1350 of deformation in lacustrine seismites (Tierras Blancas Basin, Mexico):
1351 Quaternary International, v. 219, p. 66-78.

Rodríguez-Pascua, M.A., Garduño-Monroy, V.H., Pérez-López, R., Perucha-Atienza, M.A., Isdrade-Alcántara, I, 2012, The Acambay Earthquake of 1912, revisited 100 years after: Abstract volume of the 3rd INQUA-IGCP -567 International Workshop on Earthquake Archaeology and Palaeoseismology, Morelia, México.

Rogers, R., Karason, H., van der Hilst, R., 2002, Epeirogenic uplift above a detached slab in northern Central America: Geology, v. 30, p. 1031–1034.

Santamarina, J. C., and Fam, M., 1995, Changes in dielectric permittivity and shear wave velocity during concentration diffusion: Canadian Geotechnical Journal, v. 32, p. 647-659.

Santamarina, J. C., Klein, K. A., Fam, M. A., 2001, Soils and waves. Particulate materials behavior, characterization and process monitoring: John Wiley & Sons LTD, New York, 485 p.

Saarenketo, T., 1998, Electrical properties of water in clay and silty soils: Journal of Applied Geophysics, v. 40, p. 73-88.

Siebe, C., Macías, J.L., Aguirre-Díaz, G.J., 2006, Neogene-Quaternary continental margin volcanism: A perspective from Mexico: Geological Society of America Special Paper 402, 329 p.

Soliva, R., Benedicto, A., Schultz, R. A., Maerten, L., Micarelli, L., 2008, Displacement and interaction of normal fault segments branched at depth; implications for fault growth and potential earthquake rupture size: Journal of Structural Geology, v. 30, p. 1288–1299.

Stein, S., and Liu, M., 2009, Long aftershock sequences within continents and implications for earthquake hazard assessment: Nature, v. 462, p. 87-89.

Stirling, M., Rhoades, D., Berryman, K., 2002, Comparison of earthquake scaling relations derived from data of the instrumental and reinstrumental era: Bulletin of the Seismological Society of America, v. 92, p. 812–830.

Stirling, M., Goded, T., Berryman, K., Litchfield, N., 2013, Selection of Earthquake Scaling Relationships for Seismic-Hazard Analysis: Bulletin of the Seismological Society of America, v. 103, p. 1–19.

Stubailo, I., Beghein, C., Davis, P. M., 2012, Structure and anisotropy of the Mexico subduction zone based on Rayleigh-wave analysis and implications for the geometry of the Trans-Mexican Volcanic Belt: Journal of Geophysical Research, v. 117, B05303.

Suárez, G., 1992, El sismo de Jalapa del 3 de Enero de 1920: Revista Mexicana de Ingeniería Sísmica, v. 42, p. 3–15.

Suárez, G., García-Acosta, V., Gaulon, G., 1994, Active crustal deformation in the Jalisco block, Mexico: Evidence for a great historical earthquake in the 16th century: Tectonophysics, v. 234, p. 117–127.

Suter, M., Aguirre-Díaz, G.J., Siebe, C., Quintero, O., Komorowski, J., C., 1991, Volcanism and active faulting in the central part of the Trans-Mexican Volcanic Belt, Mexico: *in* Walawender, M.J., and Hanan, B.B. (eds.), Department of Geological Sciences, San Diego State University, Guidebook 1991 Annual

Meeting Geological Society of America, p. 224-243.
Suter, M., Quintero, O., Johnson, C.A., 1992, Active faults and state of stress in the central part of the Trans-Mexican Volcanic Belt, Mexico. 1 The Venta de Bravo Fault: Journal of Geophysical Research, v. 97, p. 11983-11993.
Suter, M., Quintero, O., López, M., Aguirre-Díaz, G.J., Ferrar, E., 1995, The Acambay graben: Active intraarc extension in the Trans-Mexican Volcanic Belt: Tectonics, v. 14, p. 1245–1262.
Suter, M., Carrillo-Martínez, M., Quintero-Legorreta, O., 1996, Macroseismic study of earthquakes in the central and eastern parts of the Trans-Mexican Volcanic Belt: Bulletin of the Seismological Society of America, v. 86, p. 1952-1963.
Suter, M., López-Martínez, M., Quintero-Legorreta, O., Carrillo-Martínez, M., 2001, Quaternary intra-arc extension in the central Trans-Mexican volcanic belt: Geological Society of America Bulletin, v. 113, p. 693-703.
Urbina, F., and Camacho, H., 1913, La zona megaseismica Acambay-Tixmadeje, Estado de México, conmovida el 19 de noviembre de 1912: Boletín del Instituto Geológico de México, v. 52, p. 320-329.
Urrutia-Fucugauchi, J., and Flores-Ruiz, J., 1996, Bouger gravity anomalies and regional crustal structure in central Mexico: International Geology Review, v. 38, p. 176–194.
Van Dam, R. L., and Schlager, W., 2000, Identifying causes of ground-penetrating radar reflections using time-domain reflectometry and sedimentological analyses: Sedimentology, v. 47(2), p. 435-449.
Villamor, P., Berryman, K. R., Nairn, I. A., Wilson, K., Litchfield, N., Ries, W., 2011, Associations between volcanic eruptions from Okataina volcanic center and surface rupture of nearby active faults, Taupo rift, New Zealand: Insights into the nature of volcano-tectonic interactions: Geological Society of American Bulletin, v. 123, p. 1383–1405.
Wells, D. L., and Coppersmith, K. J., 1994, New empirical relationships among magnitude, rupture length, rupture width, rupture area, and surface displacement: Bulletin of the Seismological Society of America, v. 84, p. 974–1002.
Wesnousky, S. G., 2008, Displacement and geometrical characteristics of earthquake surface ruptures: Issues and implications for seismic hazard analysis and the process of earthquake rupture: Bulletin of the Seismological Society of America, v. 98, p. 1609–1632.
Witkind, I., J., Bradley Myers, W.B., Hadley, J.B., Hamilton, W. and Fraser, G.D., 1962, Geologic features of the earthquake at Hebgen Lake, Montana, August 17, 1959. Bulletin of the Seismological Society of America, v. 52:2, p. 163-180.
Yang, T., Grand, S.P., Wilson, D., Guzmán-Speziale, M., Gómez-González, J. M., Domínguez-Reyes, T., Ni, J., 2009, Seismic structure beneath the Rivera subduction zone from finite-frequency seismic tomography: Journal of Geophysical Research, v. 114, B01302.
Zúñiga, F. R., Figueroa-Soto, A., Ortuño M., 2011, Probabilistic estimation of

average recurrence time of damaging events at a crustal faulting regime site with low frequency of large events and lack of recorded seismicity. In proceedings of: 7th International Workshop on Statistical Seismology, Thera (Santorini), Greece.

FIGURES AND TABLES

Figure 1. Regional index map of Acambay graben (and of Figure 2) showing the geodynamic setting of the graben within the Trans-Mexican Volcanic Belt. EPR-East Pacific Rise, TR-Tehuantepec Ridge.

Figure 2. Main active faults in the central TMVB drawn on a 30 m resolution Digital Elevation Model (DEM) of the area using INEGI data (2011). The instrumental seismicity of the period 1956-2012 has been included together with the focal mechanism of the 1979 Maravatío earthquake (mb=5.3) taken from Astiz, (1980), and the epicenter of the 1912 Acambay earthquake taken from Figueroa (1970), with Ms= 6.7 according to Suter et al. (1995).

Figure 3. Simplified geologic map of the Acambay graben showing the main lithostratigraphic units and geomorphological fault traces identified within the graben. Geological mapping was done by Gerardo J. Aguirre-Díaz. Also shown are reported paleoseismological trench sites from other studies. A shaded relief derived from the 30 m resolution DEM from INEGI data (2011) is used as a background. Area zoomed in for Figure 4 is also shown.

Figure 4. Geological units and neotectonic features at the western tip of the Western Pastores fault (WPF). Locations of the sites studied (A, B and C) are marked by a white star.

Figure 5. **A)** Detailed map of the Laguna Bañí study area zoomed in from Figure 3. See Figure 4 for location. **B)** Sketch of the paleoseismological site Laguna Bañí indicating the position of the two trenches described in this study and the GPR profiles.

Figure 6. Photographs of the studied sites. **A)** View to the ESE of the southern branch of the Western Pastores fault marking the location of sites A and B. **B)** View to the East of the northern Western Pastores fault and the Laguna Bañí basin. **C)** Pastores fault zone developed on fluvial sediments at site A. **D)** Slickenlines in a fault plane found in fluvial sediments at site A. **E)** Aspect of the block and ash deposit at the Pastores fault scarp near Laguna Bañí sag pond. **F)** Fluvio-lacustrine deposits affected by a Western Pastores fault secondary fault at site A. **G)** Artificial cut at site A showing the present day soil (a), a talus deposit (b), a pyroclastic flow deposit (c), the regolith of unit d (d'), and a lahar deposit (d). The steps in the topography and the

lateral discontinuity of underlaying materials suggest the presence of two faults at depth.

Figure 7. Logs of the two trenches studied, comparison with GPR results, and legend of the exposed units. Valid radiocarbon ages are marked in blue, invalid are marked in red. **A)** Laguna West E-wall, **B)** Laguna West W-wall, **C)** Laguna East E-wall, **D)** Laguna East W-wall, **E)** GPR profile of Ruedo 2, which corresponds to the Laguna East trench section. Not all the discontinuities observed in the reflectors match with the ones observed in the trench. Note that several of the main fault zones (4.1, 4.2, 6) can be identified in the GPR profile, as well as the folds affecting the lower lacustrine units.

Figure 8. Photographs of the paleoseismological site and trench exposures. **A)** View of the Laguna East and West trenches at the toe of the main Western Pastores fault scarp. **B)** Open fractures on the basal lacustrine unit FL3, columns 36-37. **c)** Striated block in faults zone 4.1. **D)** Fault Zone 4.2, columns 3-5. **E)** Open fracture and filling in Fault Zone 5.3. **F)** Fault Zone 1.1 in the Laguna West trench E-wall, column 0. The picture was flipped for easier correlation with Log of Figure 9a.

Figure 9. South-North GPR profiles using the 900 MHz antenna and a time window of 100 ns. Vertical scale corresponds to depth with an estimated velocity of propagation of 11.34 cm/ns. Locations of profiles are indicated in Figure 5B. Lengths are variable: (A) Ruedo 1; 35 m length, (B) Ruedo 2, 37.5 m length; (C) Ruedo 3, 32 m length and (D) Ruedo 4, 25 m length. The profile (b) Ruedo 2 shows the logs of the analyzed sequences in column 9 and column 43 (out of the presented profile). The records of fault branches are indicated. Note vertical displacements in (C) Ruedo 3 profile. An overall displacement of the Ignimbrite Unit can be estimated in more than 60 cm.

Figure 10. Detailed stratigraphic and structural analysis of the Ruedo 2 GPR profile. Stratigraphic logs include the variation of grain size distribution with depth. C43 log is located out of the profile. C9 log shows a sequence of massive ashes with some weathered joints, with increasing clay content towards the top, which has been well recorded in the GPR profile. C43 log shows a mainly silty sequence of fluvial deposits overlying the grey ignimbrite; local variation of sand and clay content permitted to record the stratigraphic contacts and to estimate the propagation velocity of electromagnetic waves. The fault branch radar signature is enhanced by the lack of continuity of the identified layers.

Figure 11. Four possible scenarios for the paleoseismic sequence. The different chronologies result from two possible evaluations of the age of the samples, in combination with the interpretation of sample C03 as contemporaneous (Model 1) or reworked (Model 2), in relation to the timing of the opening of fracture F. 4.3. Model A rejects samples C8 and C6 as valid ages. Model B also rejects sample C19. Model

A 2 is considered the preferred one.

Figure 12. Compared paleoearthquake chronologies of the Pastores fault and the Acambay-Tixmadejé fault. For Pastores fault, the chronology of paleoseismic events recorded at Manto del Rio site, at the eastern tip of the WPF, are taken from Langridge et al. (2013). For the Acambay-Tixmadejé fault, the synthetic paleoearthquake history is taken from the combination of four paleoseismologicl sites studied by Langridge et al. (2000).

Table 1. Dating results for the samples collected at Laguna E and Laguna W trenches.

Table 2. Paleoseismic events defined in the analysis of Laguna East and Laguna West trenches, considering Model A 2 as the most probable chronology. The displacements, as analyzed by each fault branch during each event, have been included, and the maximum observed displacement has been marked in bold letters.

Table 3. Variations in depth of physical properties of samples used in the processing of the GPR data.

Figure 1
Click here to download high resolution image

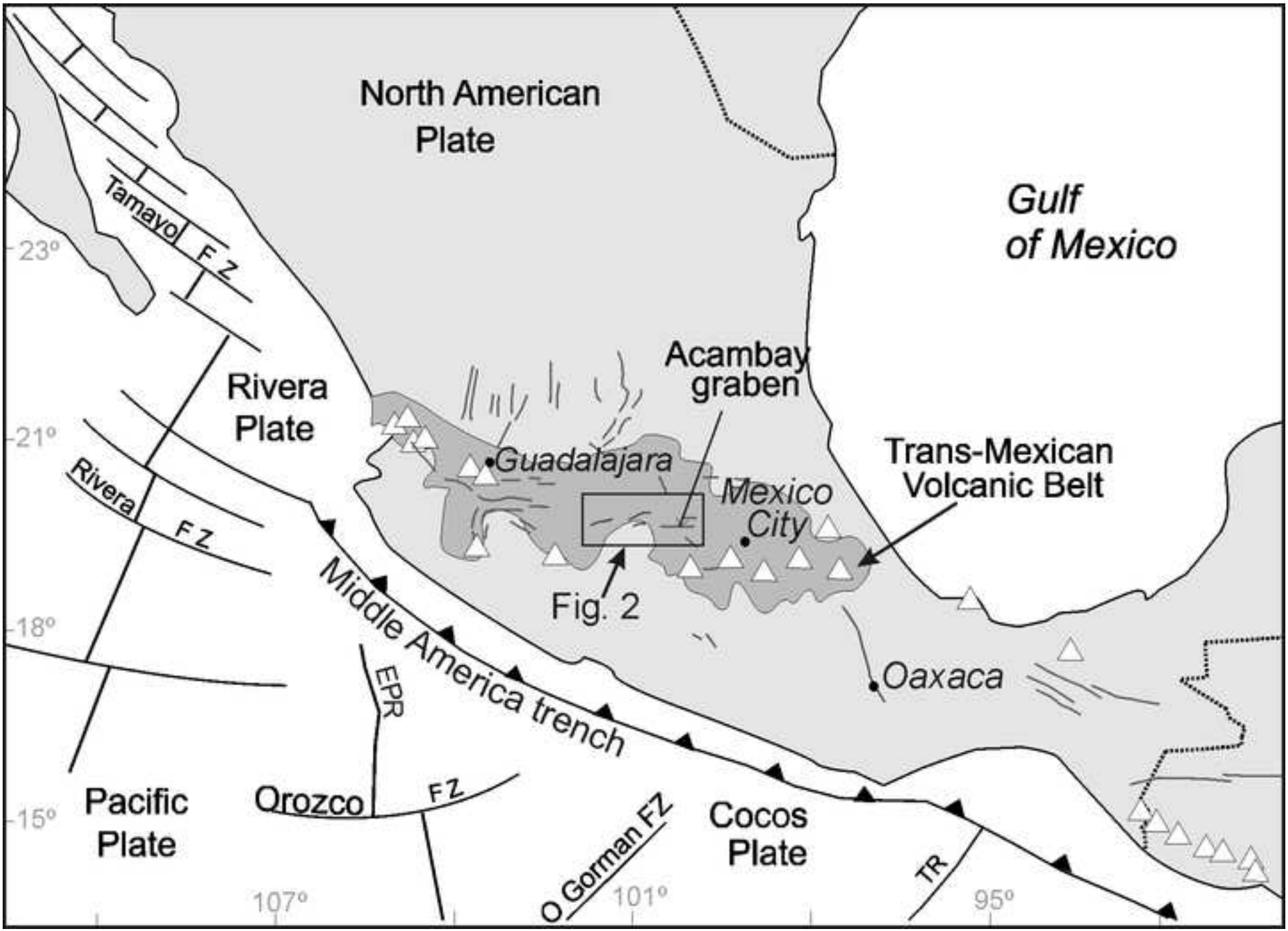

Figure 2
Click here to download high resolution image

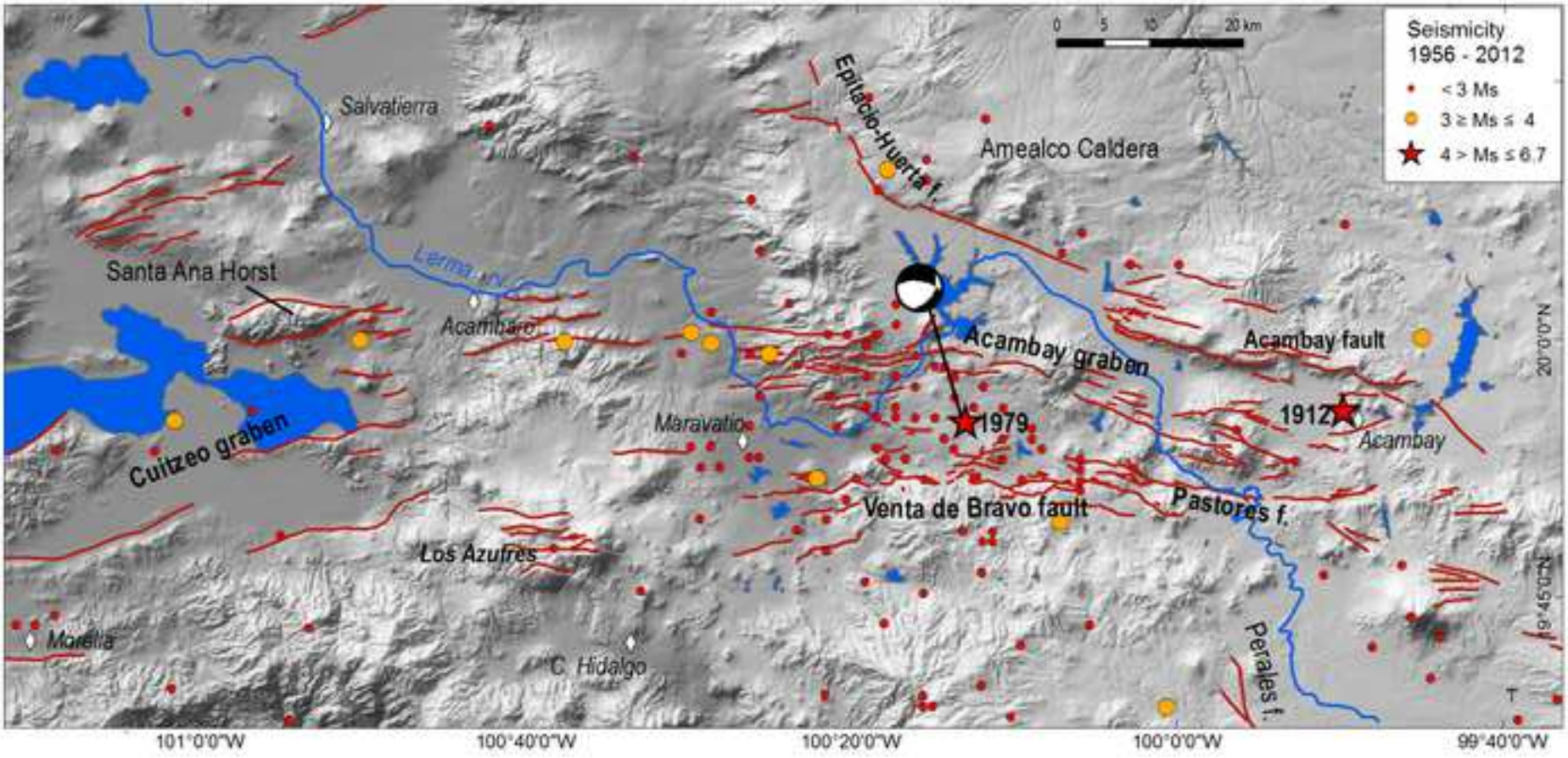

Figure 3
Click here to download high resolution image

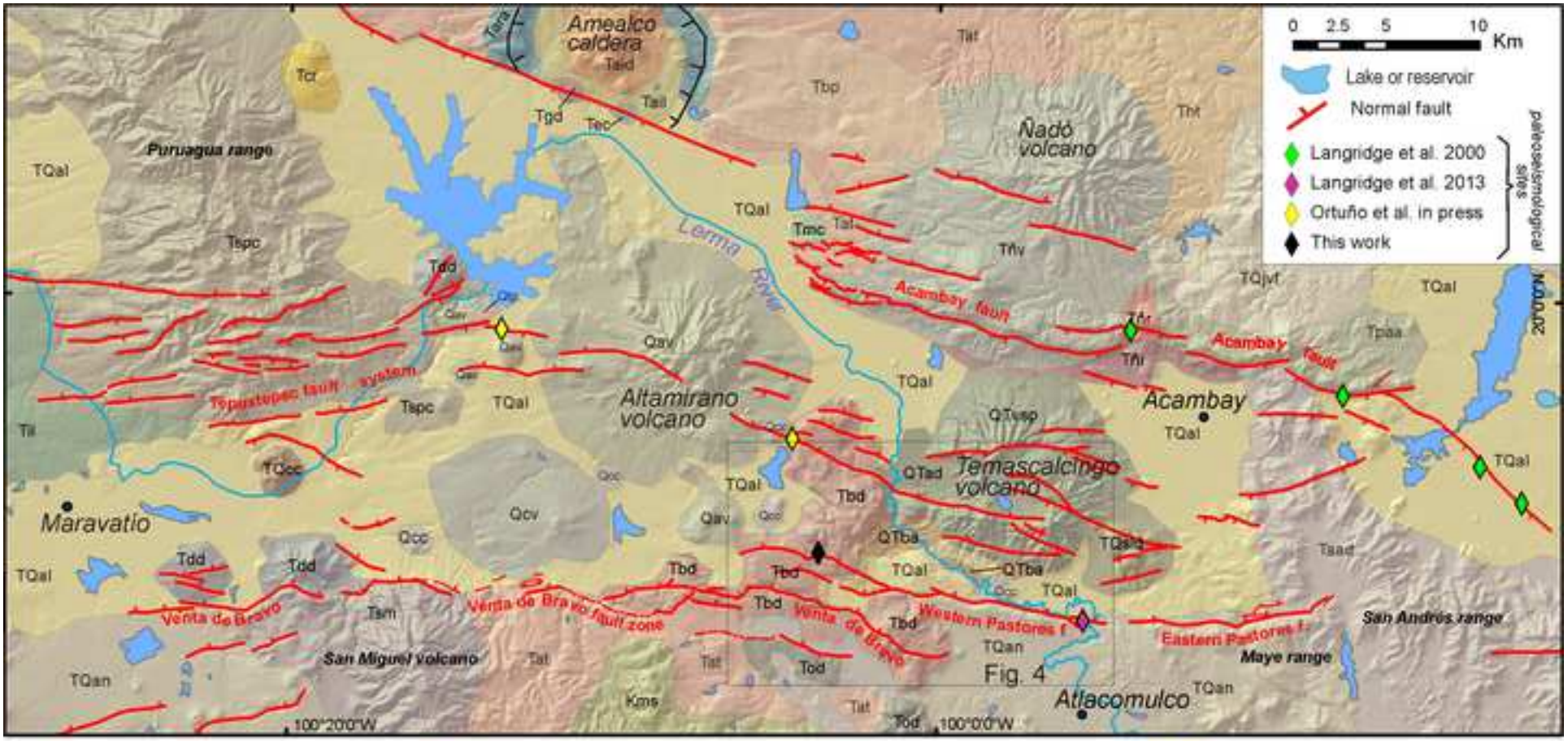

GEOLOGICAL UNITS

- TQal Plio-Qt fluvio-lacustrine deposits
- Qcc Qt cinder cone
- Qtp Qt Tepuxtepex pumice fall deposit
- Qav Qt Altamirano volcano
- Qtad Qt Temascalcingo avalanche deposit
- Qtvsp Qt Temascalcingo volcano-San Pedro caldera
- Qtba Qt Temascalcingo volcano block & ash flows
- Qcv Qt El Cereo shield volcano
- TQcc Plio-Qt cinder cone
- TQsld Plio-Qt Santa Lucía dacitic dome
- Tec Pliocene El Comal Cone (2.2 Ma)
- Tgd Pliocene Garabato dome (2.5 Ma)
- Tan Pliocene andesitic lava
- Tjvf Pliocene Jilotepec Volcanic Field (2-4 Ma)
- Tdd Pliocene dacitic dome and lavas
- Tbd Pliocene Bañi dacitic domes
- Tod Miocene El Oro dacite
- Tbp Pliocene Brick Pumice
- Tat Amealco Tuff (4.7 Ma)
- Taad Miocene Acambay andesite-dacite lavas
- Tspc Miocene Sierra Puruagua Complex
- Tit Miocene ignimbrites and lavas
- Tmc Miocene cinder cone
- Tñv Miocene Ñadó volcano
- Tñr Miocene Ñadó rhyolitic dome
- Kms Mesozoic metasediments
- Tcr Pliocene Coronita rhyolitic domes (3.5 Ma)
- Tald Amealco intracaldera domes (3.8-3.7 Ma)
- Tail Amealco caldera intracaldera lake deposits
- Tara Amealco caldera rim andesite (4.0 Ma)
- Tpaa Pliocene Peñas de Acambay andesite
- Tht Huichapan Tuff (4.2 Ma)
- TÑi Miocene Ñadó ignimbrites
- Tsm Miocene San Miguel volcano

Figure 4
Click here to download high resolution image

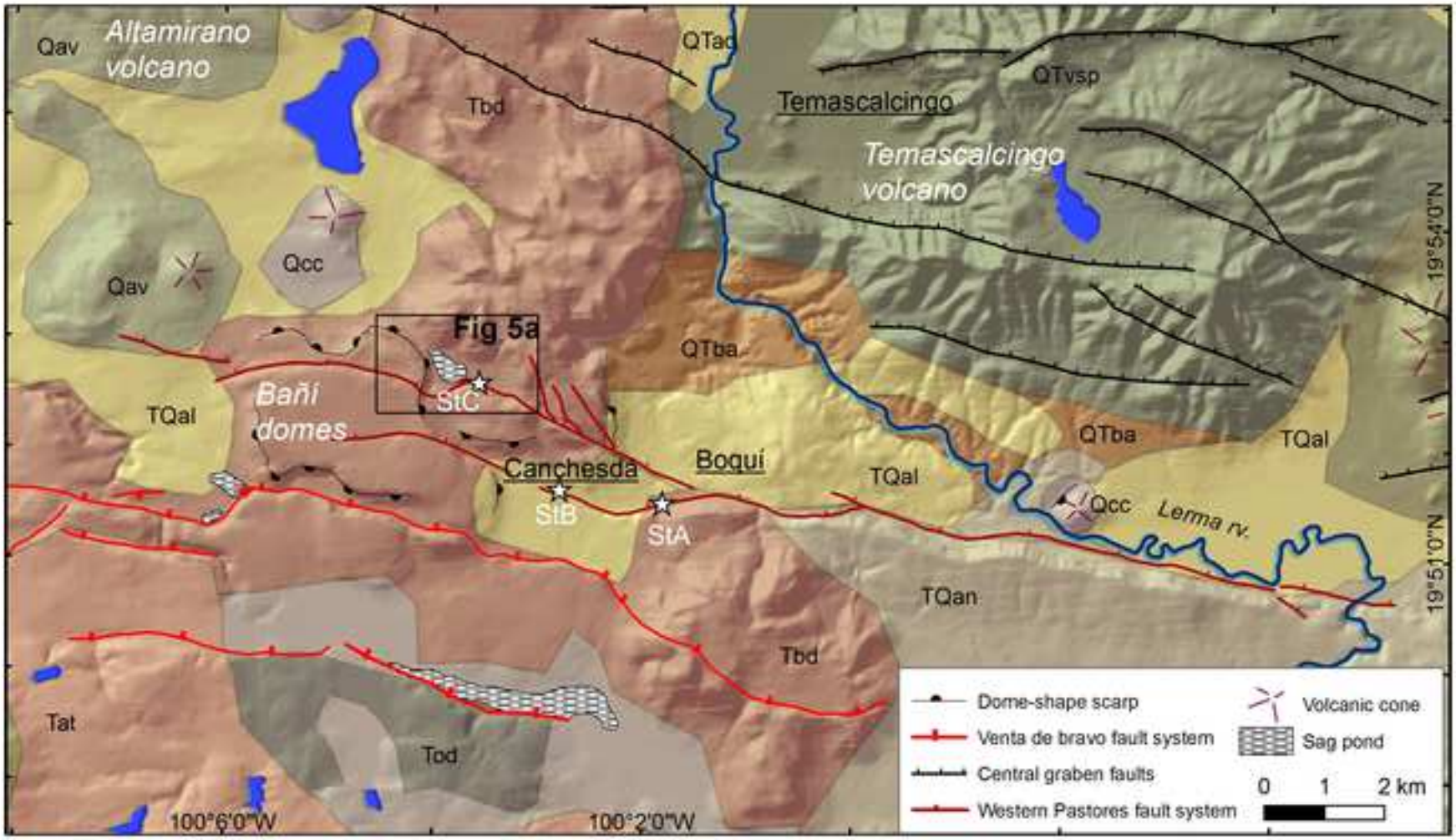

Figure 5
Click here to download high resolution image

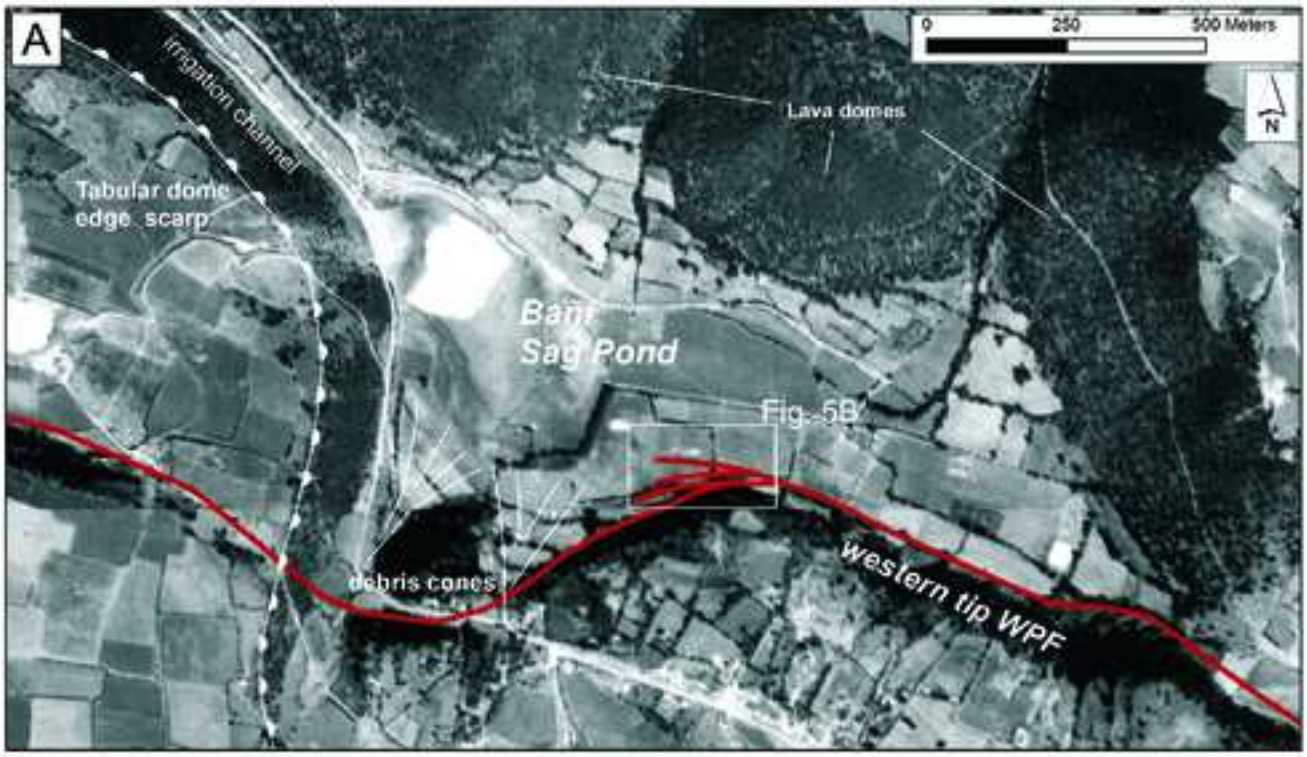

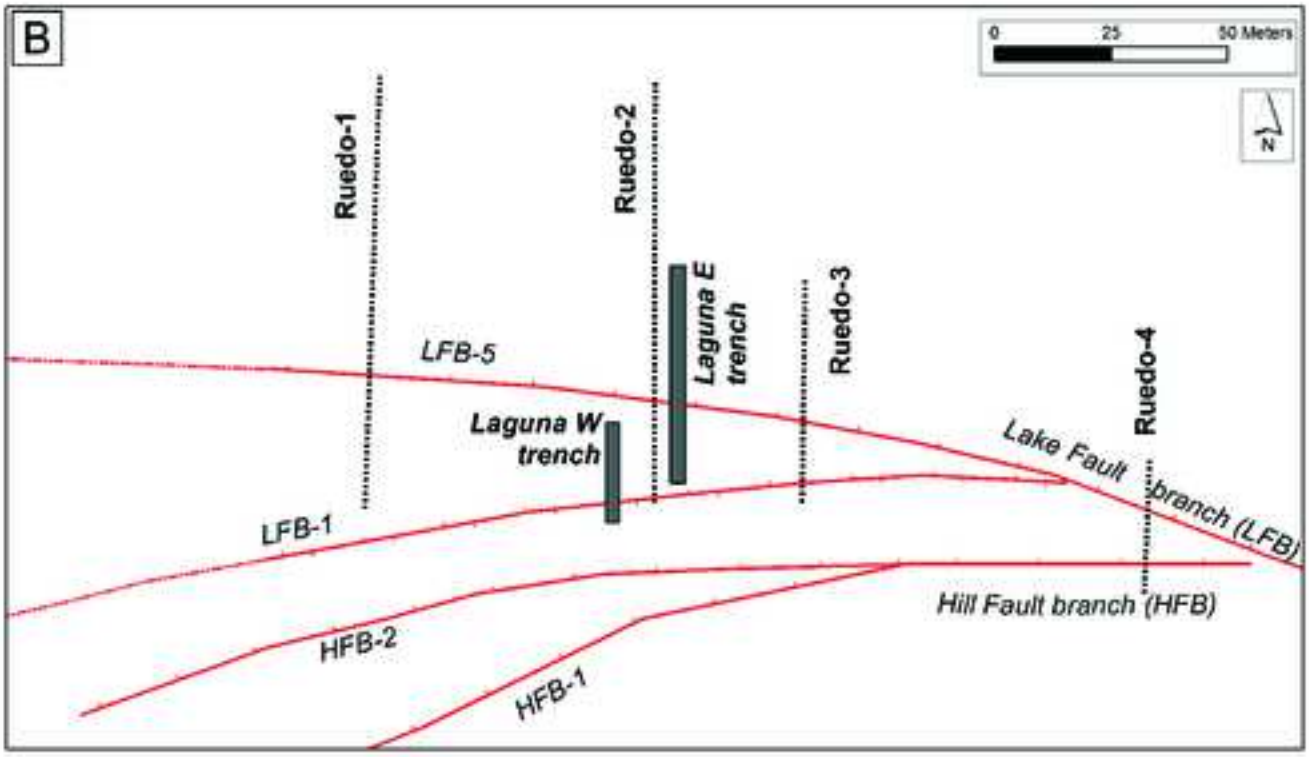

Figure 6
Click here to download high resolution image

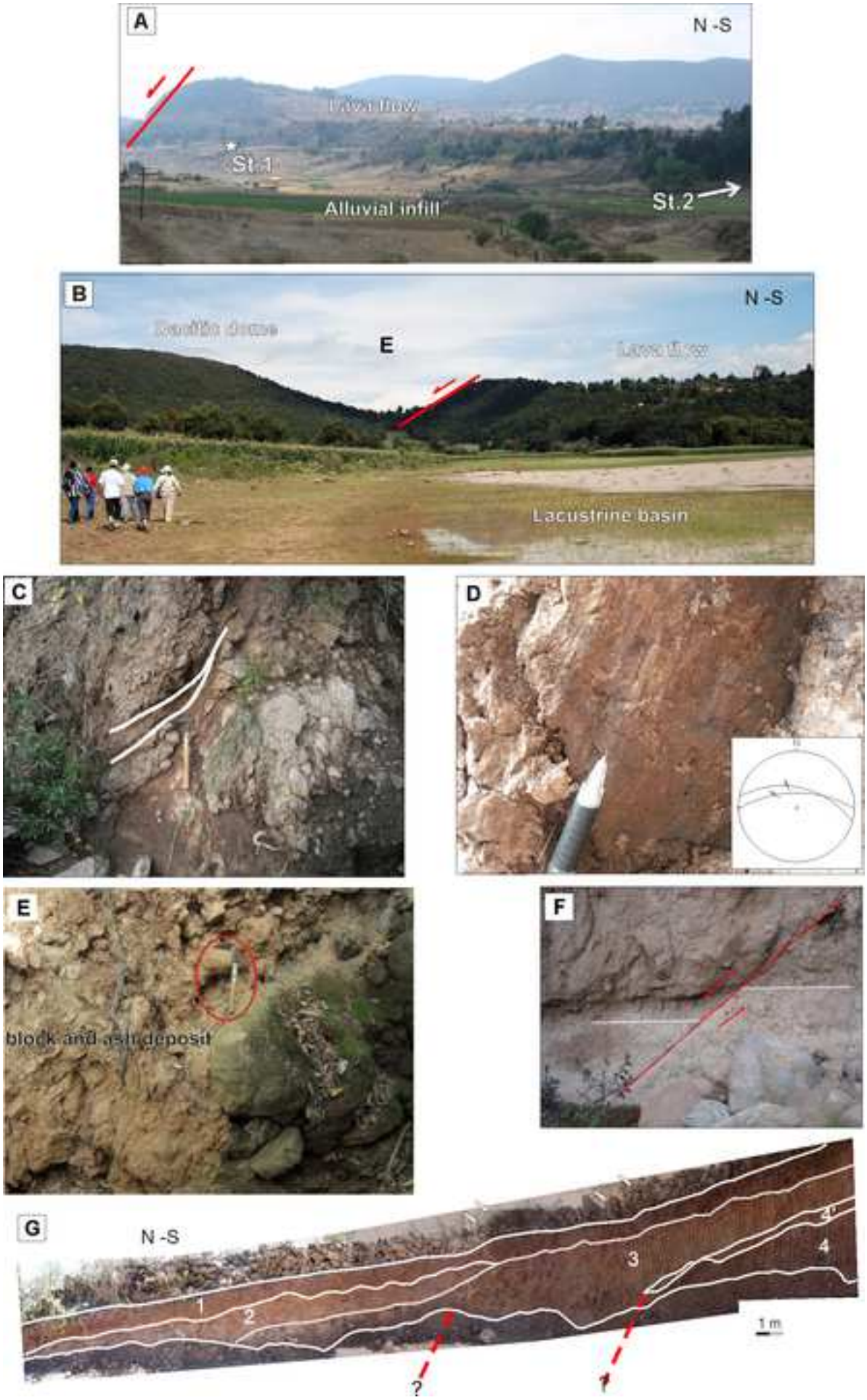

Figure 7abc

Click here to download high resolution image

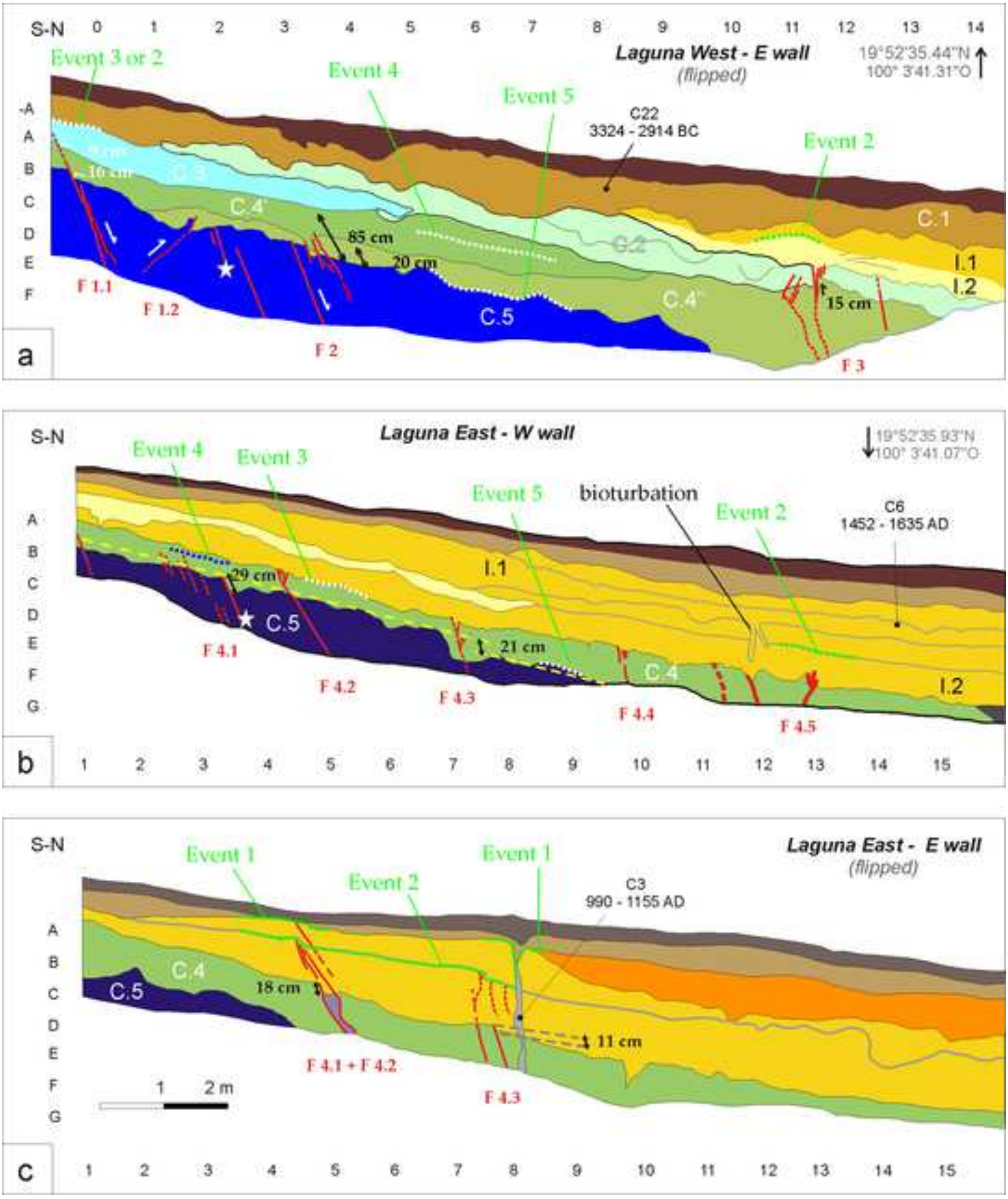

Figure 7de

Click here to download high resolution image

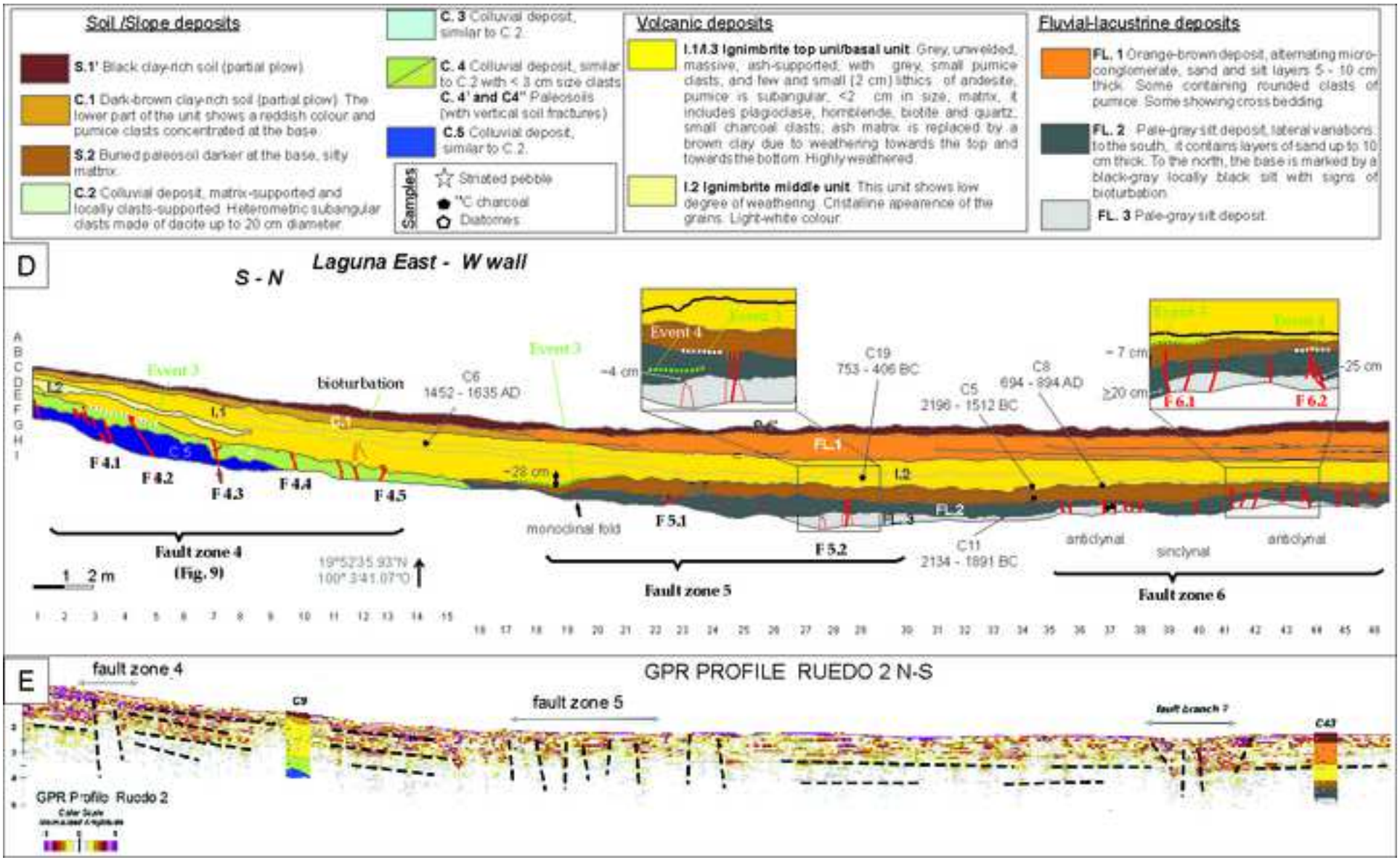

Figure 8
Click here to download high resolution image

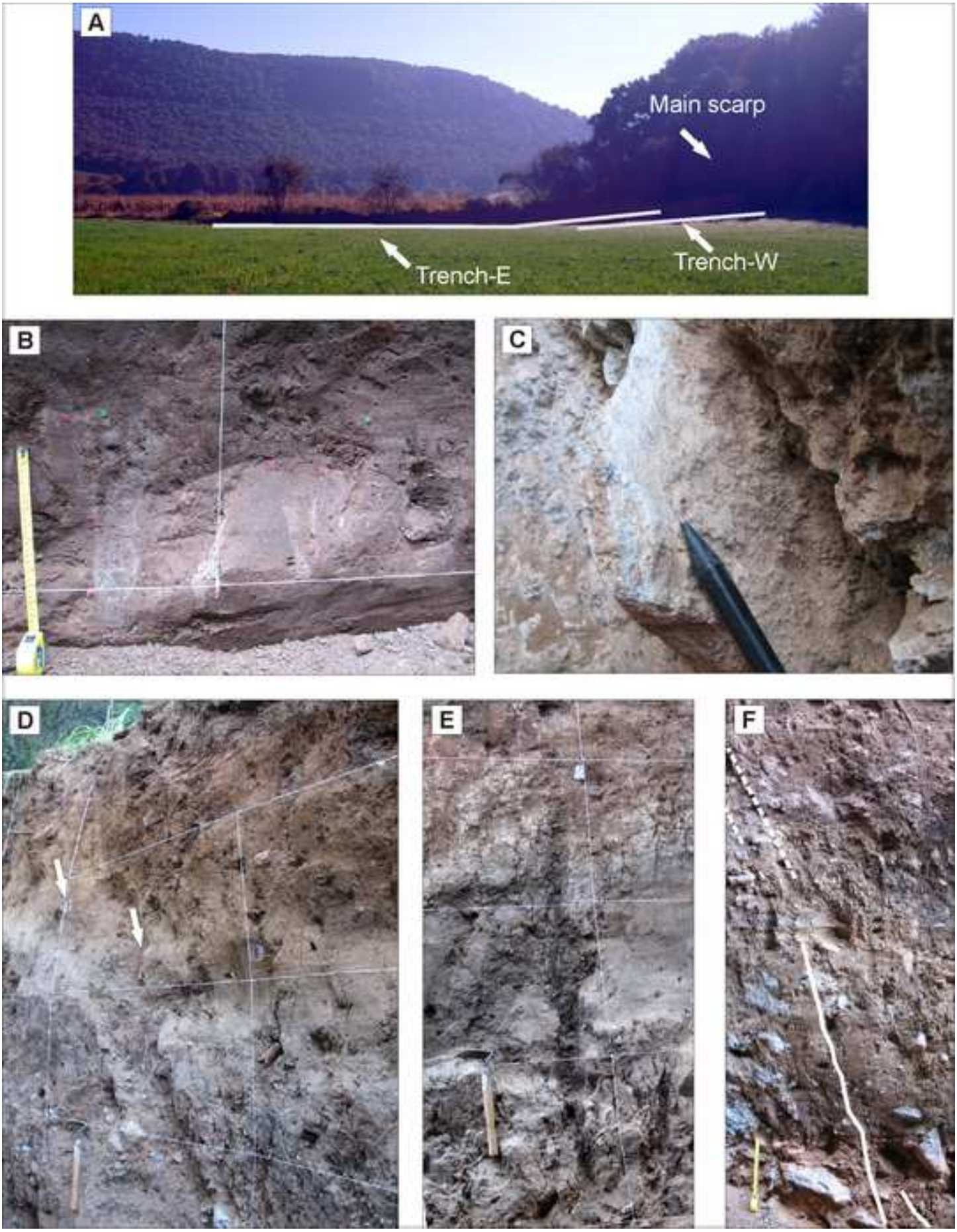

Figure 9
Click here to download high resolution image

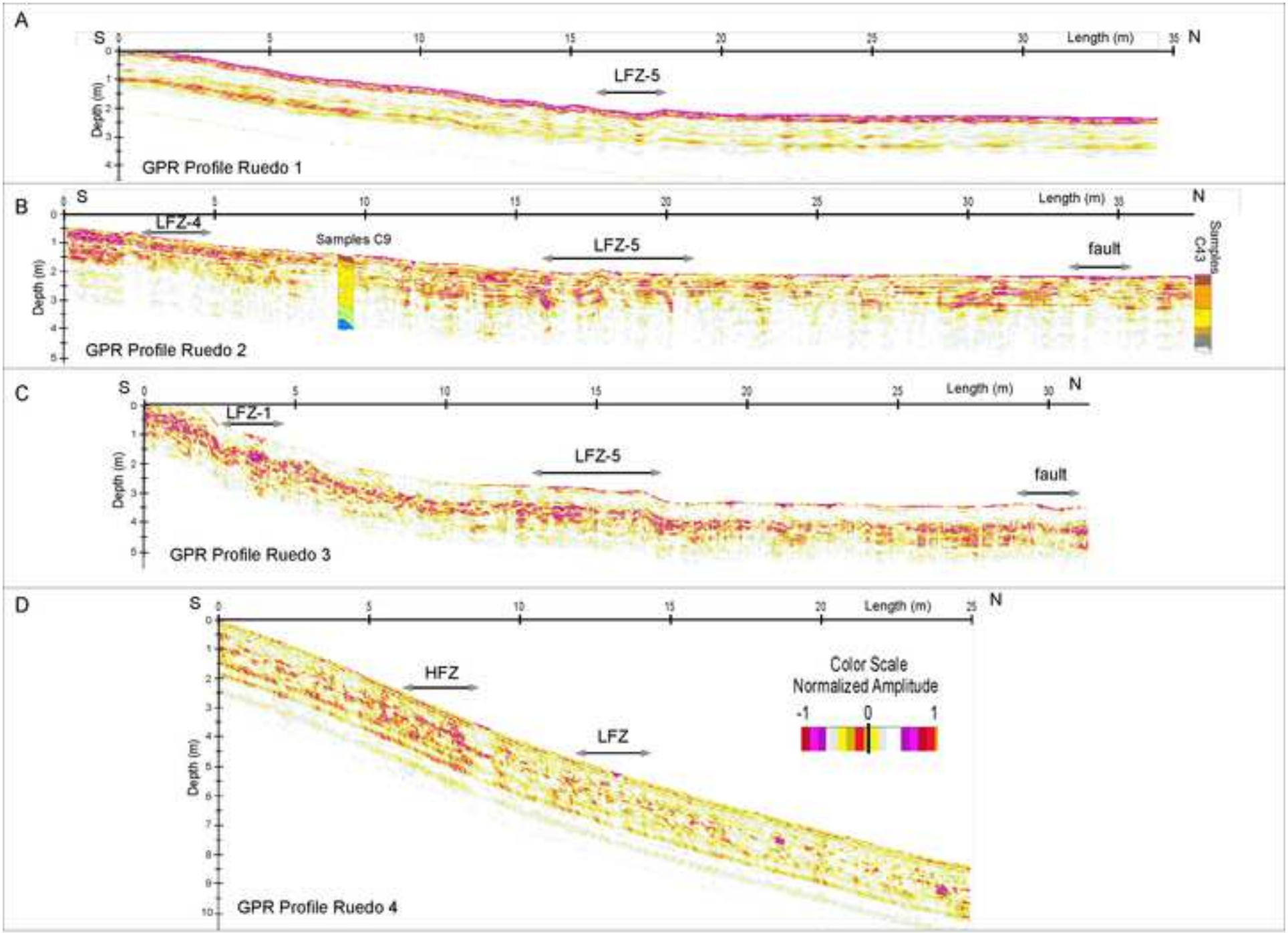

Figure 10

Click here to download high resolution image

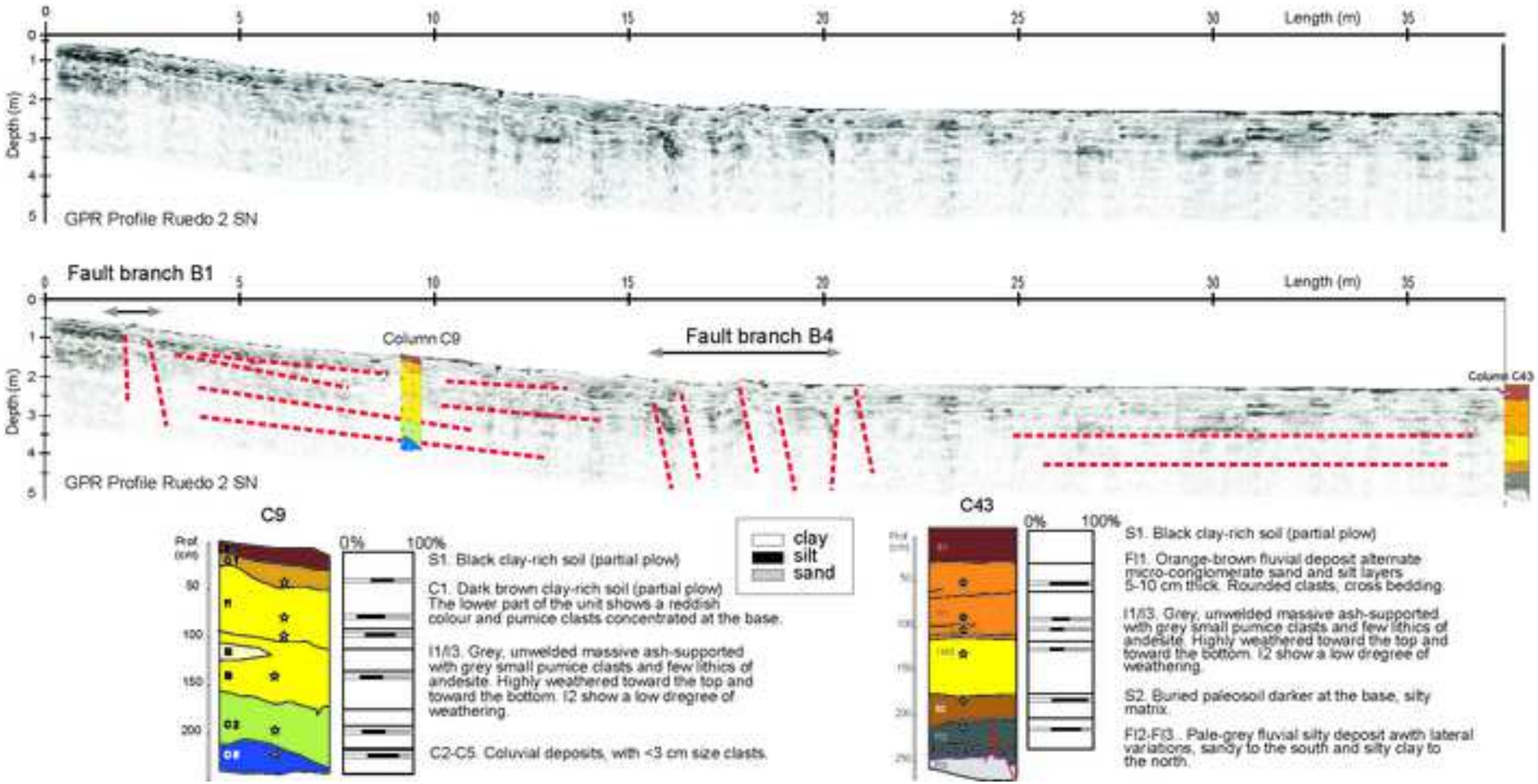

Figure 11
Click here to download high resolution image

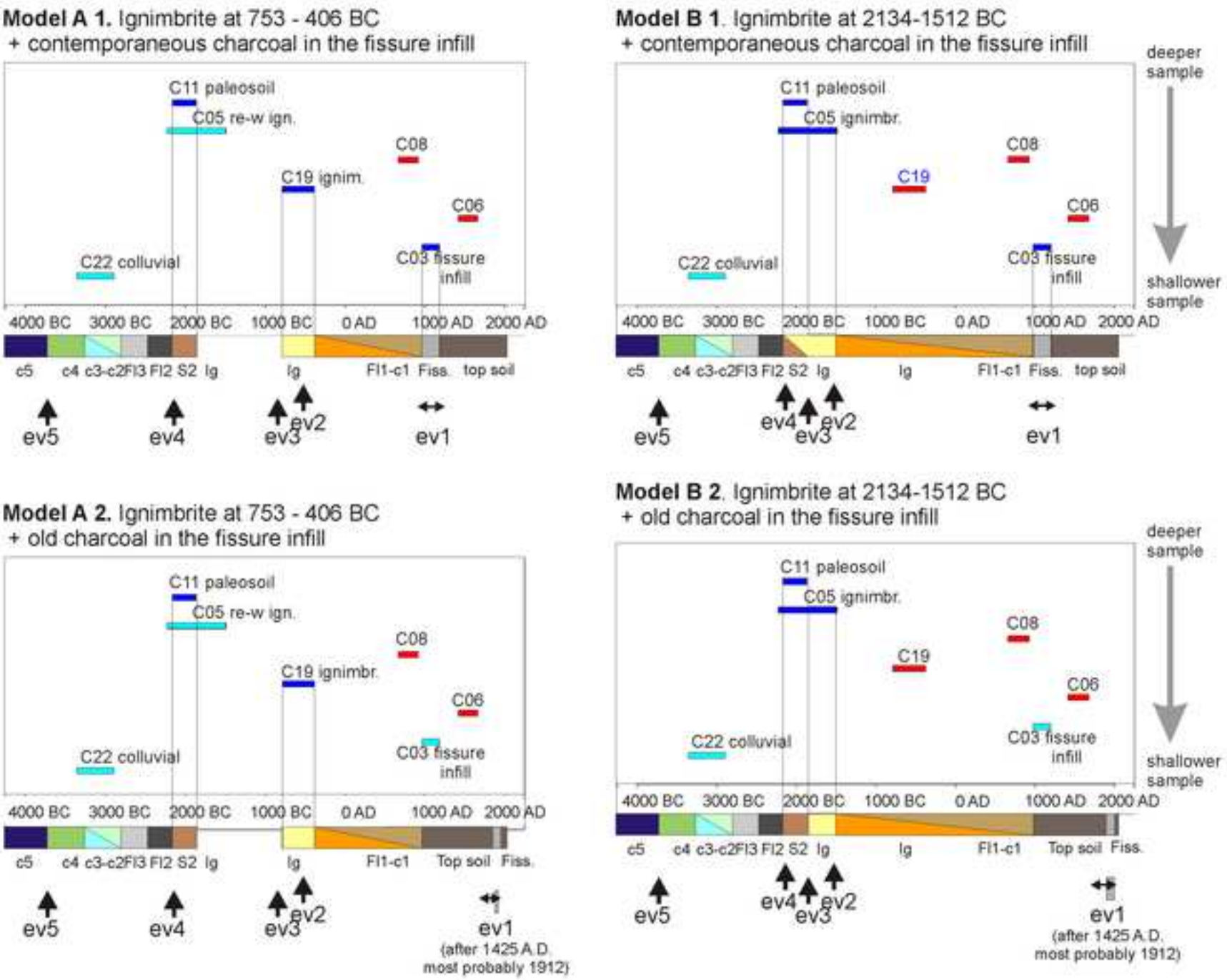

Figure 12
Click here to download high resolution image

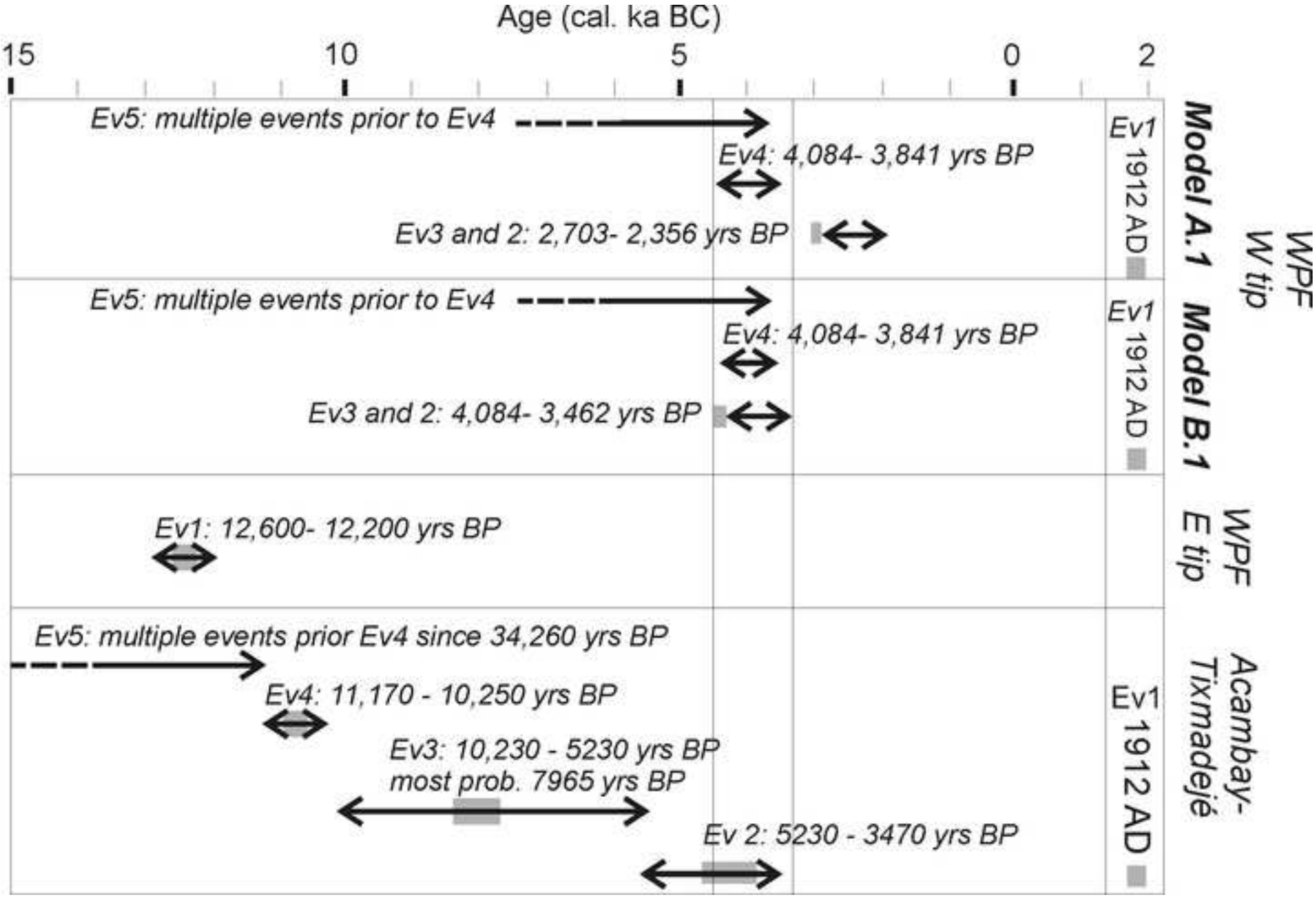

Table 1

TABLE 1. DATING RESULTS FOR THE SAMPLES COLLECTED AT LAGUNA E AND LAGUNA W TRENCHES

Sample	Radiocarbon age ^{14}C (yrs.)	Error (yrs.)	2σ Calibrated age (yrs.) from (-BC/+AD) to (-BC/+AD)		Comment	Location
C22	4410	40	-3324	-2914	Out of sequence, probably reworked	Young colluvial (unit C1)
C3	983	36	990	1155	Fracture infill	Fracture infill (Tr-1-E)
C6	356	35	1452	1635	Probably rejuvanated by edaphic bleaching	Ignimbrite (I1)
C19	2440	40	-753	-406	Most probable age of the ignimbrite	Ignimbrite (I3)
C8	1205	30	694	894	Probably rejuvanated by edaphic bleaching	Ignimbrite (I3)
C5	3500	130	-2196	-1512	Probably reworked	Ignimbrite (I3)
C11	3630	40	-2134	-1891	Age of the buried paleosoil	Paleosoil (S-2)

See Fig. 7 for location of samples

Table 2

TABLE 2. PALEOSEISMIC EVENTS DEFINED IN THE ANALYSIS OF LAGUNA EAST AND LAGUNA WEST TRENCHES, CONSIDERING MODEL A 2 AS THE MOST PROBABLE CHRONOLOGY

Event	Bracketting unit: lower/upper	Age (^{14}C yrs. BP)	Apparent displacements (cm)*	Observation
1	Within C.1	$\leq$ 990 – 1155 AD		Open fracture, fractures developed up to top layers of the ignimbrite (Laguna W-Ewall), with no clear displacement. The age of the event must be similar or younger than the fracture infill.
2	Base of the ignimbrite/FL. 1 (Laguna E-Wwall, c.18-20, c. 41-42; Laguna E-Ewall, c. 4 - 8)	753 – 406 BC	*Laguna W-Ewall*: possibly 9 (F 1); -15 (F 3); **Total max: 29** in *Laguna E-Ewall*: 18 (F 4.1 - 4,2); 11 (F 4.3); *Wwall*- 28 (gentle fold F 5).	This event closely postdates the ignimbrite deposition.
3	Immediately before Ignimbrite I.3 / FL. 2; I.2 /C.3(C.2)	≈ (753-406 BC) < 2134 – 1891 BC	*Laguna W-Ewall*: 9 (F 1, if not occurred in event 2); **Total max: - 10** in *Laguna E-Wwall*: -3 (F 5.1); -7 (F 6.1).	This event preceeds very closely the ignimbrite deposition.
4	Some time before Ignimbrite: intra C4' and intra FL 2/S2 (preferred age)	≈ 2134 – 1891 BC	*Laguna W-Ewall*: 7 (16 - 9, F 1.1), -20 (F 1.2), 20 (F 2); **Total max: 37** in *Laguna E-W wall*: 29 (F 4.1), -4 cm (F 5.2); -13 (-20 - 7 in F 6.1); 25 (19 + 6 in F 6.2).	
5	C. 4/C. 5	> 2134 – 1891 BC	**Total max: 65** in *Laguna W-Ewall*: 85 - 20 (F 2); *Laguna E- Wwall*: 21 (F. 4.3);	This is possibly a multiple-event , it creates an scarp controlling the geometry of unit C.5

* positive values: dip slip; negative values: , reverse slip

Table 3

TABLE 3. VARIATIONS IN DEPTH OF PHYSICAL PROPERTIES OF SAMPLES USED IN THE PROCESSING OF THE GPR DATA

Sample/ Unit	Depth (cm)	G (gr/cm^3)	Clay (%)	Silt (%)	Sand (%)	LL (%)	PL (%)	IP (%)	USCS
C43 6/ FL.1	63	2.50	35.33	57.88	6.79	38.20	26.11	12.09	ML
C43 5/FL.1	106	2.52	37.03	24.24	38.73	38.90	25.14	13.76	ML
C43 4/FL-1	114	2.53	31.22	23.08	45.7	33.75	22.87	10.88	ML-S
C43 3/I.1	143	2.40	37.08	59.21	3.71	42.40	27.54	14.86	ML-C
C43 2/I.3	186	2.40	37.41	52.57	10.01	38.75	27.06	11.69	ML-C
C43 1/FL.2	224	2.39	37.4	42.97	19.63	38.60	25.96	12.64	ML

Sample/ Unit	Depth (cm)	G (gr/cm^3)	Clay (%)	Silt (%)	Sand (%)	LL (%)	PL (%)	PI (%)	USCS
C9 7/C.1	52	2.5	36.02	32.66	31.32	38.30	24.55	13.75	ML
C9 6/I.1	82	2.49	20.78	39.02	40.2	35.10	25.00	9.90	ML-S
C9 5/I.1	94	2.37	31.17	43.88	24.95	35.40	24.76	10.64	ML
C9 4/I.1	144	2.48	23.66	31.61	38.73	38.25	27.65	10.60	ML
C9 3/C.5	195	2.4	26.36	33.44	40.2	27.40	19.92	7.48	ML-C
C9 2/C.6	222	2.38	36.03	45.6	18.37	38.80	26.16	12.64	ML-C

Samples collected from columns no. 9 and 43. G-Specific Gravity of Soil Solids, g/cm^3. LL-Liquid Limit, LP -Plastic Limit, IP-Index of plasticity in terms of gravimetric water content. USCS-Unified Soil Classification System.See Fig. 10 for location of samples.

Appendix A

Click here to download Supplemental file: Ortuno et al Appendix A1, A2.pdf